Editors' Suggestion

Pair-density waves, charge-density waves, and vortices in high-T_c cuprates

Zhehao Dai, Ya-Hui Zhang, T. Senthil, and Patrick A. Lee*
Department of Physics, Massachusetts Institute of Technology, Cambridge, Massachusetts, USA

(Received 3 March 2018; revised manuscript received 24 April 2018; published 14 May 2018)

A recent scanning tunneling microscopy (STM) experiment reports the observation of a charge-density wave (CDW) with a period of approximately 8a in the halo region surrounding the vortex core, in striking contrast to the approximately 4a period CDWs that are commonly observed in the cuprates. Inspired by this work, we study a model where a bidirectional pair-density wave (PDW) with period 8 is at play. This further divides into two classes: (1) where the PDW is a competing state of the d-wave superconductor and can exist only near the vortex core where the d-wave order is suppressed and (2) where the PDW is the primary order, the so-called "mother state" that persists with strong phase fluctuations to high temperature and high magnetic field and lies behind the pseudogap phenomenology. We study the charge-density wave structures near the vortex core in these models. We emphasize the importance of the phase winding of the d-wave order parameter. The PDW can be pinned by the vortex core due to this winding and become static. Furthermore, the period-8 CDW inherits the properties of this winding, which gives rise to a special feature of the Fourier transform peak, namely, it is split in certain directions. There is also a line of zeros in the inverse Fourier transform of filtered data. We propose that these are key experimental signatures that can distinguish between the PDW-driven scenario from the more mundane option that the period-8 CDW is primary. We discuss the pro's and con's of the options considered above. Finally, we attempt to place the STM experiment in the broader context of pseudogap physics of underdoped cuprates and relate this observation to the unusual properties of x-ray scattering data on CDW carried out to very high magnetic field.

DOI: 10.1103/PhysRevB.97.174511

I. INTRODUCTION

The pseudogap phase has long been considered a central puzzle in the study of the cuprate high-temperature superconductors [1]. After decades of studies, the phenomenology is well established. The pseudogap temperature is now demonstrated to signal a genuine phase transition: some form of broken crystalline symmetry has been shown to occur from ultrasound attenuation [2], second harmonic generation [3], and the anisotropy of the spin susceptibility [4,5]. Just below this temperature, neutron scattering has detected the onset of intracell magnetic moments [6] which have been interpreted in terms of orbital loop currents [7], even though this experimental finding has recently been challenged, at least in the case of YBCO [8,9]. At lower temperatures, short-range order charge-density wave (CDW) order emerges, often, but not always, suppressed by the onset of superconductivity [10–13]. In high magnetic field, the CDW order in YBCO dramatically increases its range, as seen in NMR [14–16]. X-ray scattering reveals that it is unidirectional and becomes stacked in the phase between layers [17–19]. There seem to be two coexisting distinct forms of CDW, one long ranged ordered and unidirectional, while the other is short ranged and exists in both directions. It is quite mysterious why they have the same incommensurate period. At very low-temperature, quantum oscillations have been observed, which have been interpreted as the emergence of small electronlike pockets (for a review, see Ref. [20]). Of course, the appearance of a pseudogap in the single-particle spectrum near the antinode which persists to very high temperature is what gave this phenomenon its name in the first place. The phenomenology is so rich and complicated that it seems to defy any unifying theme, leading to notions such as competing orders or intertwined order. Adding to this complexity, a recent STM experiment detected CDW with period 8a coexisting with the previously observed period-4a CDW in the halo surrounding the vortex core (a is the lattice constant) [21]. In this broader context, a key question we would like to address is this. Does this observation simply increase the complexity of the problem or is it the breakthrough that provides the key to crack open the pseudogap problem?

It should be noted that the double period CDW is expected in a scenario based on the existence of pair-density wave (PDW) when it coexists with the d-wave superconducting order. In this paper, we review different scenarios that can lead to the double period CDW and discuss the pro's and con's of each of them. Most importantly, we propose a refinement of the STM experiment which we believe can unambiguously distinguish between different scenarios, including different versions of PDWs, like canted PDW and unidirectional PDW.

A PDW is a superconductor with a pairing order parameter which is periodic in space. It was first introduced by Larkin and Ovchinnikov [22] and by Fulde and Ferrell [23] as a way to overcome the Pauli limiting effect of a magnetic field. The notion of PDW in the context of the cuprates has a long history. Himeda, Kato, and Ogata [24] found in 2002 by projected Monte Carlo studies that the PDW is the preferred ground state in the presence of stripe order. Starting from the standard

*palee@mit.edu

stripe picture [25] of a period-8 spin density wave (SDW) and a period-4 CDW, they found that the d-wave superconductor is more stable if the sign of the order parameter is reversed at the hole poor region of the CDW, leading to a period-8 PDW. We shall refer to this state as the stripe-PDW. They proposed that if the stripe-PDW are stacked perpendicular to each other from one layer to the next, the resulting state has drastically reduced Josephson coupling and may explained the disappearance of the Josephson plasma edge observed in Nd-doped $LaSr_2CuO_4$ (LSCO) [26]. Strong anisotropy in the transport properties was discovered in the $La_{2-x}Ba_xCuO_4$ (LBCO) system [27] and since that time the theory of layer de-coupled PDW and related phases has been greatly advanced [28,29]. For a review, see Ref. [30].

The next development is the introduction of a Landau theory description [28,29,31,32]. Agterberg and Tsunetsugu [31] described the coupling of PDW with various subsidiary orders such as CDW and magnetization waves. By examining the interplay between the PDW vortex and the dislocation in the CDW, they showed that it is possible to suppress the PDW order by phase fluctuations, while the subsidiary CDW order remains long ranged. Berg, Fradkin, and Kivelson [32] constructed a phase diagram using renormalization group arguments, which include regions in parameter space where the primary PDW order is destroyed while CDW and a novel charge 4e superconductor survive. Berg *et al.* [30] suggested that the stripe PDW may have a more general applicability than the low-temperature behaviors in the LBCO family, i.e., it may be behind the pseudogap phase. Part of their argument is based on the spectral property of such a unidirectional PDW. We comment that while this state produces what looks like a Fermi arc, the gap is actually small near the antinode in the direction perpendicular to the stripe orientation [30,33]. This kind of two-gap structure has difficulties with STM and ARPES data.

Stimulated by a detailed angle-resolved photo-emission (ARPES) study of the single layer cuprate Bi2201 [34], one of us [35] proposed that the unusual features of the spectra can be explained by postulating a bidirectional PDW state as the underlying state of the pseudogap. The pairing is produced by singlet pairing of electrons with momenta $K_i + p$ and $K_i - p$ where the K_i's are located at or near the Fermi surface at the antinodal points [see Fig. 1(a)]. This gives rise to a bidirectional PDW. The pair carries momenta P_1 and $-P_1$, which equal twice the momentum K near the $(\pi,0)$ antinode and are along the x axis. There is a similar pair P_2 and $-P_2$ along the y axis. There are four order parameters: Δ_{P_1}, Δ_{-P_1}, Δ_{P_2}, and Δ_{-P_2}. While Lee proposed using the idea of Amperean pairing [36] as the microscopic origin of the PDW, most of the paper was phenomenological, and explored the consequences of an assumed PDW. As such, many of the conclusions are quite general. Nevertheless, we would like to emphasize that the motivation for introducing the bidirectional PDW is fundamentally different from that for the unidirectional PDW [30,37], which is rooted in the phenomena observed in the LSCO/LBCO family at relatively low temperatures. Our view is that the recently discovered CDW, which survives up to 150 K are, is distinct from the stripe physics associated with LSCO/LBCO. The wave vector decreases with increasing doping, whereas the stripe wave vector increases linearly up to about 0.125 doping and saturates, following the Yamada plot [38]. For YBCO, the period is incommensurate and close to 3, very different from the period-4 CDW associated with 1/8 doping in LSCO. Finally, there is no sign of the SDW that is intertwined with the stripes. As phenomenology the bidirectional PDW produces the pseudogap at the antinodes and the Fermi arcs near the nodes. (Strictly speaking, these are the electronlike segments of closed orbits made up of Bogoliubov quasiparticles.) It explains why the gap closes at the end of the Fermi arcs with states moving up from lower energy, while a CDW-generated gap will necessarily close by a state coming down in energy. As opposed to conventional pairing, the spectrum is not particle-hole symmetric at each k point, which explains why the momentum of the minimum gap is shifted away from the original Fermi surface. In addition, a CDW at wave vectors $Q = 2P_1$ and $2P_2$ naturally emerges as a subsidiary order. The states at the Fermi arcs play two important roles. First, they greatly suppress the superfluid density and therefore the phase stiffness, so that the PDW is subject to strong phase fluctuations over most of the phase diagram in the H-T plane. Secondly, the normal state gives rise to a linear term in the entropy, which lowers the free energy and stabilizes it at finite temperatures, even if it is not the true ground state. In addition, in the superconducting state, a CDW with period P_1 and $P_2(= Q/2)$ naturally appears if the PDW phase is pinned to that of the d-wave pairing and reference was made to an STM experiment on YBCO where CDW at Q and $Q/2$ have been reported [39,40], where $Q = 0.28(2\pi/a)$ matches what is now determined by x-ray scattering.

We should point out that other workers have also associated PDW with the pseudogap phenomenon. Zelli, Kallin, and Berlinsky [41] used the quasiparticle orbits produced by an unidirectional PDW order to produce quantum oscillations. A related proposal was recently made by M. Norman and J. C. Davis [42]. We will comment on this below. Yu *et al.* [43] have interpreted their high magnetic field phase diagram in terms of a possible PDW. Two distinct pair fluctuation lifetimes have been reported in tunneling experiments, possibly indicative of the presence of two kinds of superconductors [44]. Other papers consider a PDW with the same wave vector and on equal footing as the CDW and are less relevant to the present discussion [45,46].

Next, an interesting observation was made by Agterberg *et al.* [47] that by shifting the momenta K from the zone boundary line, a new state is formed where the PDW carries momentum P_1 and a momentum P_1' which is not equal to $-P_1$ and similarly for P_2' [see Fig. 1(a)]. We shall refer to this state as canted PDW, referring to the canting of the pairing momenta as seen in Fig. 1(a). Agterberg *et al.* [47] showed that this state breaks time-reversal and inversion symmetry, but preserves the product and that this is precisely the symmetry of the loop current model of Varma [7], which has been used to interpret the neutron scattering data.

Advanced numerical methods applied to the t-J models have found evidence for stripe-PDW as a competing state [48]. Interestingly, the energy is found to be quite insensitive to the hole filing per period, in contrast to the original stripe picture which strongly prefers half a hole per period.

In the remaining of this paper, we address the adequacy of each of the following scenario's as the explanation of

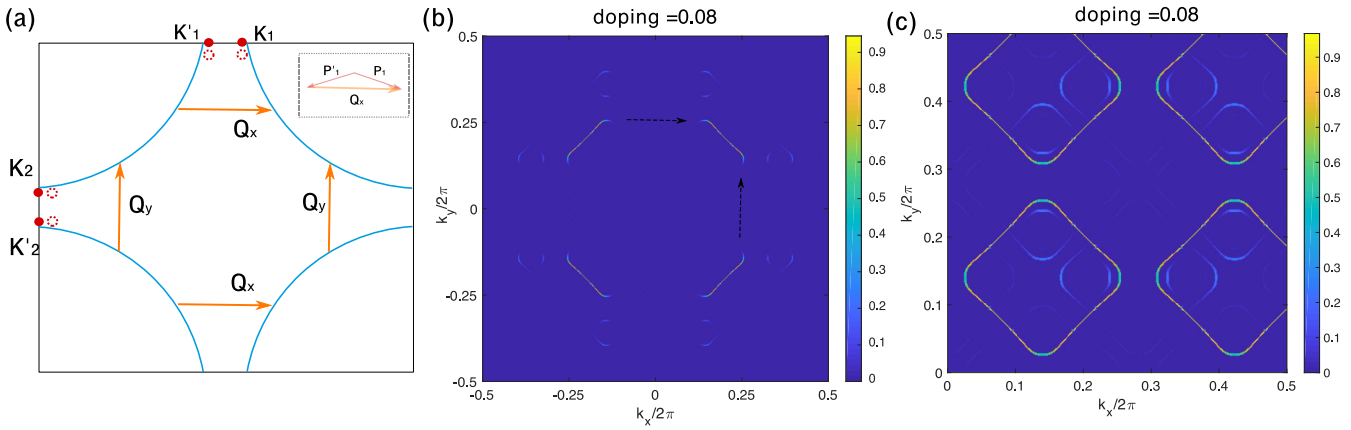

FIG. 1. Band structure of Bogoliubov quasiparticle and possible Fermi pockets in a PDW state. (a) An illustration of the bare Fermi surface, CDW momenta, and PDW momenta. CDW momenta Q_x and Q_y are shown as yellow arrows. PDW momenta are $P_1 = 2K_1$, $P_1' = 2K_1'$ in x direction, and $P_2 = 2K_2$, $P_2' = 2K_2'$ in y direction. CDW is a subsidiary order of PDW, its momenta $Q_x = P_1 - P_1'$, $Q_y = P_2 - P_2'$. We consider two scenarios: (1) K_i and K_i' are located right at BZ boundary (solid red dots). $P_1 = -P_1' = Q_x/2$, $P_2 = -P_2' = Q_y/2$. (2) K_i and K_i' are slightly shifted (dotted red circles); P_1 and P_1' have a small y component, as shown in the inset figure (the small y component is exaggerated). (b) Electron weight on the Fermi pocket of Bogoliubov quasiparticle. We used the band structure in Appendix A, CDW momentum $Q_x = Q_y = 0.28(2\pi/a)$ measured in Ref. [13], PDW order parameter $\Delta_{Q/2} = 45$ meV, no explicit CDW order parameter in mean-field Hamiltonian, and plotted the electron weight at the Fermi energy and each momentum k in the BZ (for details, see Appendix A). The electron weight is large on four "arcs" in the nodal direction. The antinodal direction is gapped out by PDW. (c) Details of the reconstructed electronlike pocket after BZ folding caused by CDW. We plotted the total electron weight at momenta up to Q_x and Q_y. This pocket is formed by four segments with electron weight $> 80\%$. It has the same shape as the Harrison-Sebastian pocket. Physically, there is only one pocket, others are its copy shifted by Q_x and Q_y. we only show the upper right quadrant of the BZ.

the double period CDW, put in the broader context of the pseudogap phenomenology. (1) The $Q/2$ CDW is the primary order, while the Q CDW is subsidiary. (2) The $Q/2$ PDW is a competing order, or an example of intertwined order where several order parameters such as PDW, CDW, SDW, and d-wave pairing are intimately related to each other. In this picture, the PDW exists only in the vortex halo and vanishes outside. (3) The PDW is the primary order, the mother state that exists at a high-energy scale and lurks behind a large segment of the phase diagram in the temperature/magnetic field plane. In order to explain the pseudogap at the antinodes, the PDW is assumed to be bidirectional. While its order is destroyed by phase fluctuations, there are several subsidiary orders that emerge at lower temperatures, which account for the observed complexity of the phase diagram. We shall also include a discussion of the canted PDW. Throughout this paper we assume the PDW to be bidirectional.

A recent paper by Wang *et al.* [49] addresses issues related to PDW in the STM experiment and there are similarities and differences with the present work. They consider the d-wave superconductivity and PDW as competing states inside the vortex halo and construct a sigma model description combining the two orders. They focus their calculations to unidirectional PDW. They argue against the persistence of PDW outside the vortex halo. As such their picture is closer in spirit to scenario (2) as outlined above.

II. RECENT STM RESULTS ON PERIOD-8 DENSITY WAVE

First, we give a short summary of the recent low-temperature STM experiment in $Bi_2Sr_2CaCu_2O_8$ [21]. The doping is about 0.17. At zero field patches of 4a CDW are observed. These appear locally unidirectional and have d form factors. The correlation length is very short, about twice of the lattice spacing. At a finite field of 8.25 T, by subtracting off the zero field data, period-4a and period-8a CDWs are revealed in the "halo" region around the vortex core. These appear to be bidirectional and have s-wave form factors. The signals are symmetric when the voltages are reversed. We distinguish bidirectional from "checkerboard" order, which consists of local patches of unidirectional stripes. From the widths of the Fourier transform peaks, the correlation length of the 8a and 4a CDW is about 8a and 4a, respectively, comparable to their wavelengths. By examining the signals that are odd upon reversing the voltage, another 4a CDW is found which has d form factors. Its correlation length is about 5a and it is unidirectional, running in the same direction from vortex to vortex.

Purely on symmetry grounds, the observation of period-8a bidirectional charge order in the presence of a background superconductor implies that there are also period-8 modulations in the pair order parameter. Specifically, if the Fourier component $\rho_{Q/2}$ of the density at a wave vector $Q/2$ is nonzero, then it implies a nonzero Fourier component $\Delta_{Q/2} \sim \Delta_d \rho_{Q/2}$ in the pairing order parameter (where Δ_d is the order parameter for the standard d-wave superconductor). An important question then is whether the observed period-8 modulations are driven primarily by the pinning of soft fluctuations of $\rho_{Q/2}$ (and $\Delta_{Q/2}$ is a subsidiary) or whether the driver is pinning of soft fluctuations of $\Delta_{Q/2}$ (and the observed $\rho_{Q/2}$ is a subsidiary). We will call the former CDW-driven and the latter PDW-driven. Clearly, this is not a symmetry-based distinction and it is natural to wonder if the question is meaningful at all. However, we will argue in this paper that there are, in fact, two distinct

possibilities for the observed period-8 charge order which have distinct experimental signatures. It is natural to associate these two distinct possibilities with the (looser) distinction between CDW-driven and PDW-driven mechanisms.

III. BASIC FEATURES OF BIDIRECTIONAL PDW

In this section, we explore the implications of the PDW-driven scenario, and contrast it with the CDW-driven scenario. We will particularly emphasize the two distinct structures of the period-8 charge order and their experimental distinctions.

A. PDW with long-range order

The new CDW recently found in $Bi_2Sr_2CaCu_2O_8$ has a momentum close to $2\pi/8$, half of the momentum of the well-known short-range CDW at zero field. In the PDW-driven scenario, we consider a bidirectional PDW order with the same momentum that is roughly the momentum between tips of the bare Fermi surface in the antinodal direction [35]. A bi-directional PDW state with such a momentum is previously proposed by one of the authors [35]. Following this proposal, we write down a mean-field Hamiltonian:

$$\begin{aligned} H = &\sum_{k,\sigma} \epsilon_k c^\dagger_{k,\sigma} c_{k,\sigma} \\ &+ \sum_k \Delta^*_{P_1}(k) c_{k,\uparrow} c_{-k+P_1,\downarrow} + \Delta^*_{P'_1}(k) c_{k,\uparrow} c_{-k+P'_1,\downarrow} \\ &+ \sum_k \Delta^*_{P_2}(k) c_{k,\uparrow} c_{-k+P_2,\downarrow} + \Delta^*_{P'_2}(k) c_{k,\uparrow} c_{-k+P'_2,\downarrow} + \text{H.c.} \end{aligned} \tag{1}$$

We used the notation $P_1 = 2K_1$, $P'_1 = 2K'_1$—as shown in Fig. 1(a)—K_1 and K'_1 are located at or near the Fermi surface at antinodal points, generically incommensurate with the BZ; similarly, $P_2 = 2K_2$, $P'_2 = 2K'_2$. The four PDW order parameters generate CDW order ρ_{Q_x} and ρ_{Q_y} in second-order perturbation even though we do not include them explicitly in the Hamiltonian:

$$\rho_{Q_x} \sim \Delta_{P_1} \Delta^*_{P'_1},\ \rho_{Q_y} \sim \Delta_{P_2} \Delta^*_{P'_2}. \tag{2}$$

We associate this subsidiary CDW as the well-known short-range CDW at zero field; it has momenta $Q_x = P_1 - P'_1$, $Q_y = P_2 - P'_2$, with magnitude $Q \simeq 2\pi/4$ in the recent STM experiment. In principle, we can also add CDW in (1,1) direction, e.g., $\rho \sim \Delta_{P_1} \Delta^*_{P'_2} + \ldots$. However, this CDW is absent in the recent STM experiment; we explain the reason in detail in the next section.

Naively, one may expect that if the PDW has local d form factor, the CDW generated by Eq. (2) has s form factor. This argument is not generally correct, because s and d form factor for a finite-momentum order parameter has no sharp symmetry distinction [50].

It is a local property, which is not captured by the long-wavelength description of a Landau order parameter. In fact, when we solve our mean-field Hamiltonian with only d wave PDW as input, the CDW that emerges at Q is predominantly d wave. In view of the experimental observation of s symmetry CDW near the vortex core, this may simply indicate that the mean-field theory is not adequate to give a microscopic description. Nevertheless, we want to convey the message that this result shows that it is entirely possible that a d-wave CDW can emerge as a subsidiary order.

We define the common phases $\theta_{P,x}$, $\theta_{P,y}$ and relative phases ϕ_x, ϕ_y of the PDW order parameters, and the phases of Q CDW order parameters as

$$\begin{aligned} &\Delta_{P_1} = |\Delta_{P_1}| e^{i(\theta_{P,x}+\phi_x)},\ \Delta_{P'_1} = |\Delta_{P'_1}| e^{i(\theta_{P,x}-\phi_x)}, \\ &\Delta_{P_2} = |\Delta_{P_2}| e^{i(\theta_{P,y}+\phi_y)},\ \Delta_{P'_2} = |\Delta_{P'_2}| e^{i(\theta_{P,y}-\phi_y)}, \\ &\rho_{Q_x} = |\rho_{Q_x}| e^{i\gamma_x},\ \rho_{Q_y} = |\rho_{Q_y}| e^{i\gamma_y}, \end{aligned} \tag{3}$$

As shown in Eq. (2), $\gamma_x = 2\phi_x$ and $\gamma_y = 2\phi_y$ are the phase difference between PDW order parameters, hence the phases of the subsidiary CDW order parameter [51]; they are proportional to the shift of density wave pattern in real space. On the other hand, $\theta_{P,x}$ and $\theta_{P,y}$ carry charge 2 under external electromagnetic field; when coexist with uniform d-wave superconductivity $|\Delta_d| e^{i\theta_d}$, the relative phases $\theta_{P,x} - \theta_d$ and $\theta_{P,y} - \theta_d$, together with ϕ_x and ϕ_y determines the spatial pattern of new CDW orders with momenta P_1, P'_1, P_2, and P'_2, which are close to or equal to $Q/2$.

We consider two scenarios: (1) K_i and K'_i, $i = 1,2$ are located at the boundary of BZ, shown as solid red dots in Fig. 1(a): $2K_1 = -2K'_1 = P_1 = -P'_1 = Q_x/2$, $2K_2 = -2K'_2 = P_2 = -P'_2 = Q_y/2$; (2) K_i and K'_i are slightly shifted, shown as dashed red dots. The shifts in momenta can be either positive or negative, giving a Z_2 order parameter in each direction. We refer to this scenario as canted PDW. This possibility was discussed in Ref. [47] in relation with loop current. It has a potential ability to account for T-reversal breaking and nematicity. Regarding the recent STM experiment, these two scenarios give similar predictions. We focus on the first scenario and comment on the second when necessary.

Unlike the pairing in a conventional superconductor, where electrons forming a Cooper pair have opposite momenta and opposite velocity, this finite-momentum pairing groups electrons with momenta $K_i + \delta k$ and $K_i - \delta k$ (similarly, $K'_i + \delta k$ and $K'_i - \delta k$) and it has a strong effect only when these two momenta are both close to the Fermi surface. As a result, it opens a gap only in the antinodal direction [shown in Fig. 1(b)], and leaves a gapless surface of Bogoliubov quasiparticle in the nodal direction.

Since PDW and CDW are generically incommensurate to the BZ, we need to set a cutoff in momentum-space calculation. It was previously reported in Ref. [35] by one of the author that a five-band model describing the mixing of c_k, $c^\dagger_{-k+P_1}$, $c^\dagger_{-k+P'_1}$, c_{k-Q_x}, and c_{k+Q_x} (similarly in y direction) produce Bogoliubov pockets with predominant electron weight on one side and predominent hole weight on the other side. In order to capture the effect of BZ folding caused by the subsidiary CDW, we increase the cutoff, and include the mixing among $c_{k+mQ_x+nQ_y}$ for m, n up to ± 2 (for details, see Appendix A). We used the Hamiltonian in Eq. (1), the band structure in Appendix A, CDW momentum $Q = 0.28(2\pi/a)$ measured in Ref. [13], PDW order parameter with d-wave form factor

$$\begin{aligned} &\Delta_{\pm Q_x/2}(k) = 2\Delta(\cos(k_x \mp Q_x/4) - \cos(k_y)), \\ &\Delta_{\pm Q_y/2}(k) = 2\Delta(\cos(k_x) - \cos(k_y \mp Q_y/4)), \end{aligned} \tag{4}$$

with $\Delta = 45$ meV, and no explicit CDW order parameter in the mean-field Hamiltonian. We found that, the electronlike part of the four Bogoliubov pockets recombine into a predominantly electronlike pocket, similar to the Harrison-Sebastian pocket [shown in Figs. 1(b) and 1(c)].

We believe that these pockets formed by mainly electronlike segments will give rise to quantum oscillations. The reason is that while the Bogoliubov quasiparticles do not carry fixed charges, they carry a well defined current, because the holes are moving in the opposite direction. In these orbits, all the segments are electron like. In a semiclassical picture, a wave packet will travel in real space along a close contour that encloses the magentic flux. By the Onsager argument, we can expect quantum oscillations. In contrast, there are many closed orbits made up of segments that are part electron and part hole like [42]. If we draw an arrow corresponding to the current, we find that at the corners where the electronlike and the holelike segments meet, they both run into the corner and undergo Andreev scattering, i.e., the currents go into the condensate. In this case, even though the orbits look closed in momentum space, the wave packets do not form closed orbit in real space, because part of the current goes into the condensate. Then Onsager's argument no longer applies. For this reason we think it is unlikely that such orbits give rise to quantum oscillations, but only a detailed calculation can tell us the answer for sure. Analogous issues arise with the Fermi surface formed by Bogoliubov quasiparticles in a d-wave superconductor coexisting with loop current order. In that problem, detailed calculations [52,53] indeed show that at $T = 0$ such a Fermi surface does not lead to quantum oscillations. We note that Zelli *et al.* [41] claimed that oscillations corresponding to such orbits exist, but their conclusion is based on an approximate calculation. We believe this issue should be revisited.

Another point is that the PDW is a superconductor and in principle we should include vortices when we introduce the magnetic field. We provide the following argument. First, it is known that quantum oscillations appear in the mixed state with a frequency which is the same as the same pockets in the normal state [54]. This has been confirmed by numerical calculations with randomly pinned vortices in a d-wave superconductor as long as the correlation length is not too short [55]. Of course, to address quantum oscillations, we need to think about a metallic state that emerges from fluctuations of a PDW ordered state. We will leave this problem aside in the present paper.

We would like to mention that as we increase doping, the 4 electron pockets [56] in Fig. 1(c) touch each other. In some parameter range, the Fermi surface topology changes, and a hole pocket forms in the middle. This Lifshitz transition is predicted for Hg1201 at 10% doping in Ref. [13], and for YBCO at a larger doping. However, distinguishing subtle changes of Fermi surface topology is beyond the scope of the current paper.

B. Static short-range PDW

In this section, we discuss the situation where a short-range PDW coexists with d-wave superconductivity. We focus on the setup of the recent STM experiment where a period-8 density wave was found in the vortex halo of a d-wave superconductor. To simplify the discussion, we consider the simplest scenario: $P_1 = -P_1' = Q_x/2$ and $P_2 = -P_2' = Q_y/2$. We have four PDW order parameters: $\Delta_{\pm Q_x/2}$ and $\Delta_{\pm Q_y/2}$.

We consider the following couplings between PDW, d-wave, and CDW order parameters in a Landau theory in translation-invariant systems. We can write them in momentum space as

$$\Delta F = -a\rho_{Q_x}\Delta^*_{Q_x/2}\Delta_{-Q_x/2} - b\rho_{Q_x}\left[\Delta_d^2\Delta^{*2}_{Q_x/2}+\Delta_d^{*2}\Delta^2_{-Q_x/2}\right] - c\rho_{Q_x/2}[\Delta_d^*\Delta_{-Q_x/2} + \Delta^*_{Q_x/2}\Delta_d] - \ldots, \quad (5)$$

where a, b, and c are real coupling constants. For simplicity, we write down only couplings in x direction. Couplings in y direction are similar. These momentum-space couplings are conceptually helpful, but the strong breaking of translation symmetry introduced by the vortex core brings in new physics that is better captured by a real-space analysis.

Before we start, it is important to note that what the experimentalists found is not long-range PDW or CDW. Instead, an STM experiment identified a static short-range charge order that lives only inside the vortex halo, with apparent correlation length comparable to its wavelength. Theoretically, a "short-range order" naturally fluctuates with time; the existence of static short-range order raises many questions—what pins the phases of the order parameters?—why does it appear only in vortex halo? One may tend to think of a phase competition between uniform d-wave superconductivity and PDW, so that the latter may be greatly enhanced near the vortex core. However, a phase competition alone does not explain why the short-range order is static.

The answer of these questions may lie in the following observation: just like the way spatial inhomogeneity pins short-range CDW, a spatial pattern of superconductivity close to the vortex core pins a short-range PDW. This static PDW then extends to a larger region with radius defined by its correlation length ξ_P. Outside ξ_P, there is still a PDW amplitude fluctuating with time, but the time average decays exponentially.

For concreteness, we choose the origin to be the center of the vortex, (r,θ) to be the polar coordinate, (x,y) to be the Cartesian coordinate, and write down the following ansatz for the amplitude of d wave and PDW:

$$\Delta_d(\mathbf{r}) = |\Delta_d(r)|e^{i\theta_d}e^{i\theta}, \quad (6)$$

$$\Delta_{\mathrm{PDW}}(\mathbf{r}) = 2|\Delta_{Q_x/2}|e^{-r/\xi_P}e^{i\theta_{P,x}}\cos(Qx/2+\phi_x) + 2|\Delta_{Q_y/2}|e^{-r/\xi_P}e^{i\theta_{P,y}}\cos(Qy/2+\phi_y), \quad (7)$$

where $|\Delta_d(r)| = r/\sqrt{r^2+r_{\mathrm{core}}^2}$. $e^{i\theta}$ encodes the 2π phase winding of d-wave amplitude. We have three length scales. The radius of the vortex core: $r_{\mathrm{core}} \simeq 3a$, the period of PDW, $4\pi/Q \simeq 8a$, and the radius of vortex halo, where field-enhanced CDWs are found: we identify the halo size as $r_{\mathrm{halo}} \sim \xi_P \sim 4\pi/Q$. A usual Landau theory with slowly-varying order parameters implicitly assumes that $r_{\mathrm{core}} \gg 4\pi/Q, \xi_P \gg 4\pi/Q$. However, we are in the opposite limit: $4\pi/Q \sim \xi_P > r_{\mathrm{core}}$.

Since ξ_P and $4\pi/Q$ are close to each other, and they are one order of magnitude larger than the lattice constant, we do not separate the exponential decay of order parameters $\Delta_{\pm Q_x/2}$ ($\Delta_{\pm Q_y/2}$) from the oscillatory part $\cos(Qx/2+\phi_x)$ [$\cos(Qy/2+\phi_y)$], as in a usual Landau theory. Instead, we

take the ansatz in Eqs. (6) and (7), and write down their couplings in real space together with charge-density profile $\rho(r)$:

$$\begin{aligned}\Delta F = -\int \{ & a\rho(\mathbf{r})\Delta_{\mathrm{PDW}}(\mathbf{r})\Delta^*_{\mathrm{PDW}}(\mathbf{r}) \\ & + b\rho(\mathbf{r})[\Delta_d^2(\mathbf{r})\Delta^{*2}_{\mathrm{PDW}}(\mathbf{r}) + \Delta_d^{*2}(\mathbf{r})\Delta^2_{\mathrm{PDW}}(\mathbf{r})] \\ & + c\rho(\mathbf{r})[\Delta_d^*(\mathbf{r})\Delta_{\mathrm{PDW}}(\mathbf{r}) + \Delta_d(\mathbf{r})\Delta^*_{\mathrm{PDW}}(\mathbf{r})] \\ & + s[\Delta_d^*(\mathbf{r})\Delta_{\mathrm{PDW}}(\mathbf{r}) + \Delta_d(\mathbf{r})\Delta^*_{\mathrm{PDW}}(\mathbf{r})]\} d^2\mathbf{r}. \quad (8)\end{aligned}$$

We would like to remind the readers again that this free energy is not a Landau free energy in the usual sense, since we include the oscillatory part of PDW explicitly in $\Delta_{\mathrm{PDW}}(\mathbf{r})$.

The last term in Eq. (8): $-s\int \Delta_d^*(\mathbf{r})\Delta_{\mathrm{PDW}}(\mathbf{r})d^2\mathbf{r} + \mathrm{c.c.}$ is the lowest-order symmetry-allowed term that describes the phase locking between PDW and d-wave order parameter near a vortex core. In the case of spatially slowly varying order parameters, this term usually vanishes because of momentum mismatch, e.g., if the d-wave superconductivity has uniform amplitude. However, close to the vortex core, the rapid changing of d-wave amplitude strongly breaks translation symmetry. Furthermore, the phase winds by 2π around the core, and near the core the winding is sufficiently rapid that it can phase match the finite wave-vector of the PDW. As a result, the PDW is pinned to match the spatial pattern of the vortex core so that free energy is minimized.

Because of the phase winding, d-wave amplitude changes sign across the origin and the overlap integral is optimized when PDW has the form $\sin(Qx/2)$, which also changes sign at the origin. Thus ϕ_x and ϕ_y are pinned to be $-\pi/2$. Then the overall phase, $\theta_{P,x} = \theta_d$, $\theta_{P,y} = \pi/2 + \theta_d$, is pinned so that the overlap is a positive real number. This pinning mechanism completely fixes the phases of PDW; a simple calculation of the overlap integral indicates the pinning is very effective in the vortex core. For details, see Fig. 2.

Of course, at the length scale of ten lattice constants, everything except a microscopic model is merely an oversimplified illustration. Nonetheless, we believe this simple illustration captures the underlying physics of phase-locking between d-wave and various PDW order parameters. This pinning mechanism is effective exactly because $4\pi/Q > r_{\mathrm{core}}$ in the cuprates. In the opposite limit, the d-wave order parameter changes slowly. According to a usual Landau theory, this coupling cancels out. In the remaining part of this section, we discuss the consequences of this phase-locking on subsidiary charge order. We confirmed these consequences by an exact diagonalization study in the next section.

Note that PDW does not have a vortex. Since PDW lives only in small patches, vortices are not required [57], and it is energetically favorable to not have vortices in the PDW-driven scenario.

This PDW order generates various CDWs in the vortex halo:

(1) bidirectional $Q/2$ CDW. According to Eqs. (5)–(8), it has the following amplitude in real space:

$$\rho_\alpha(\mathbf{r}) = F(r)\cos(\theta + \theta_d - \theta_{P,\alpha})\cos(Q_\alpha \cdot \mathbf{r} + \phi_\alpha), \quad (9)$$

where $\alpha = x, y$, $Q_\alpha = Q_x, Q_y$ and $F(r) \sim 2c|\Delta_d(r)\Delta_{Q_\alpha/2}|e^{-r/\xi_P}$. The most interesting feature is that, apart from normal plane-wave factor, there is an additional

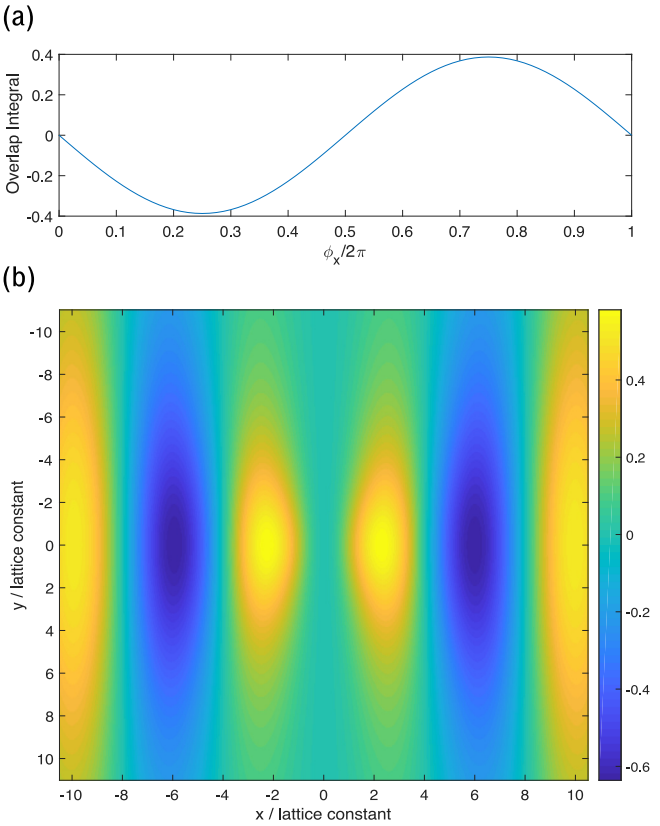

FIG. 2. (a) Overlap integral $\int \Delta_d^*(\mathbf{r})\Delta_{\mathrm{PDW}}(\mathbf{r})d^2\mathbf{r}$ as a function of ϕ_x, for $\theta_x = 0$. We have set their maximum amplitude to 1 for both $\Delta_d(\mathbf{r})$ and $\Delta_{\mathrm{PDW}}(\mathbf{r})$, and we normalize the integral by the overlap of PDW with itself inside the vortex core of radius $3a$. ϕ_x is pinned to $3\pi/2$. The large overlap implies the real-space pattern of PDW matches the pattern of d-wave vortex core almost perfectly at $\phi_x = 3\pi/2$—its amplitude is reduced only because d-wave amplitude is reduced in the vortex core. (b) The integrand $\Delta_d^*(\mathbf{r})\Delta_{\mathrm{PDW}}(\mathbf{r})$ as a function of $\mathbf{r}$ near vortex core, for $\phi_x = 3\pi/2$ and $\theta_x = 0$. Outside the vortex core, the integrand alternates between positive and negative because of momentum mismatch. However, within the first period of PDW in the center, the integrand is always positive, giving a large overlap. This is because the d wave and PDW both change sign across the origin. The d-wave changes sign due to 2π phase winding, and PDW change sign because of the $\sin(Qx/2)$ factor.

factor $\cos(\theta + \theta_d - \theta_{P,\alpha})$ depending on the polar angle. A choice of the relative angle $\theta_d - \theta_{P,\alpha}$ selects a special angle along which $\rho_\alpha(\mathbf{r})$ vanishes. We point out that the pinning mechanism we discussed predicts that the amplitude ρ_x vanishes in the vertical direction, when $\theta \sim \pm\pi/2$, while the amplitude ρ_y vanishes in the horizontal direction, when $\theta \sim 0, \pi$. This choice restores C4 symmetry. Physically, this new feature originates from the 2π winding of d-wave order parameter. We can identify two contributions to $\rho_{Q/2}$: $\Delta_d^*\Delta_{Q/2}$, which carries -1 dislocation, and $\Delta_d\Delta^*_{-Q/2}$ which carries $+1$ dislocation. The interference of these two terms gives rise to a nodal direction in real space. This is an important prediction in PDW-driven scenario. On the contrary, in a CDW-driven scenario, it is energetically favorable to put the dislocation in the PDW amplitude, and the CDW amplitude is rather featureless. In the next section, we discuss the same

feature in Fourier space, and propose follow-up experiments to distinguish PDW-driven and CDW-driven scenarios.

(2) Q CDW. According to Eq. (5) there are two contributions:

$$\rho_Q^A \sim a\Delta^*_{-Q/2}\Delta_{Q/2}, \tag{10}$$

which we call CDW_A, and

$$\rho_Q^B \sim b\left(\Delta_d^{*2}\Delta^2_{Q/2} + \Delta_d^2\Delta^{*2}_{-Q/2}\right), \tag{11}$$

which we call CDW_B, which we can think of as a harmonic of $\rho_{Q/2}$. CDW_A does not rely on the phase-locking between d wave and PDW; it is already pinned to be static short-range CDW by impurities at zero magnetic field, and it persists above T_c. On the other hand, a static CDW_B relies on the phase locking. Similar to $Q/2$ CDW, it is a superposition of $+2$ dislocation and -2 dislocation, and it exists only in vortex halo. In the case of spatially uniform PDW and CDW order, there is no distinction between the two. However, in a spatially inhomogeneous situation such as what we encounter near the vortex core, there is a physical distinction. For example, CDW_A may be extended in space while CDW_B may be localized near the vortex core. In this case, the two CDWs may have different local form factors, such as d or s wave. These form factors may in turn determine which one prefers to be bidirectional or unidirectional, because the coefficient of the quartic term that couples the amplitudes of the x and y oriented CDW may be different. In the STM data, there already appear to be two kinds of CDW's, one pinned to the vortex core and one which already exists at zero filed. We will make further use of this distinction in later discussions.

Naively, one would expect a CDW with momentum $(Q/2, Q/2)$ appears in the second order—in real space, this term may show up in the contribution $\rho(\mathbf{r}) \sim a\Delta^*_{\mathrm{PDW}}(\mathbf{r})\Delta_{\mathrm{PDW}}(\mathbf{r})$. However, the pinning in the vortex core requires

$$\Delta_{\mathrm{PDW}}(\mathbf{r}) \sim e^{i\theta_d}(\sin(Qx/2) + i\,\sin(Qy/2)), \tag{12}$$

$$\Delta^*_{\mathrm{PDW}}(\mathbf{r})\Delta_{\mathrm{PDW}}(\mathbf{r}) \sim \sin^2(Qx/2) + \sin^2(Qy/2), \tag{13}$$

and the cross term $\sin(Qx/2)\sin(Qy/2)$ with momenta $(\pm Q/2, \pm Q/2)$ cancels out due to the $\pi/2$ relative phase. As a consequence, there is no $(2\pi/8,2\pi/8)$ CDW in the leading order. In the fourth order, such a CDW is generated by the term $\Delta_d^{*2}(r)\Delta^2_{\mathrm{PDW}}(r)$, but the amplitude is weak and subject to a broadening effect given by dislocations. The absence of $(2\pi/8,2\pi/8)$ CDW is previously discussed in Ref. [31]. It was pointed out that in the uniform case when PDW does not have a vortex, the relative phase between PDW in x and y direction determines whether $(2\pi/8,2\pi/8)$ CDW is present or not. If the phase is zero, it is present, while if it is $\pi/2$, bond currents are generated, producing a flux density wave at the same wave-vector instead. This flux density wave will be discussed in great detail in a later section. In the uniform case, it is not known which phase is preferred. In our case, we find that in the presence of a vortex, the phase choice $\pi/2$ is energetically favorable, therefore $(2\pi/8,2\pi/8)$ CDW is absent in leading order. On the contrary, in CDW-driven scenario, naively, the $(2\pi/8,2\pi/8)$ CDW is comparable to the $(2\pi/4,0)$ CDW. The absence of a $(2\pi/8,2\pi/8)$ Fourier peak in STM data is an evidence favoring PDW-driven scenario.

Next, we would like to comment on the correlation length of PDW in the recent STM experiment. In PDW-driven scenario, as discussed above, the $Q/2$ CDW has 2π phase winding around the vortex core. A simple calculation shows that this phase winding broadened the Fourier peak by roughly a factor of 2. Thus the intrinsic correlation length of $Q/2$ CDW and PDW should be close to 16 lattice constants, a little smaller than the half of the distance between neighboring vortex core.

We end this section with some comments on the implications if a canted PDW is present. While the CDW generated by Eq. (2) retains the wave vector Q along the x and y axes, the double period CDW generated by the analog of the third term in Eq. (5) now has wave vectors P and P'. Similarly, its harmonic generated by the analog of the second term in Eq. (5) has wave vectors $2P$ and $2P'$. It is worth noting that we now have two distinct CDWs and the difference between A- and B-type CDWs is now a sharp one that can be made even in a uniform system. A second point is that there is now an additional pinning mechanism. The term $(\Delta_d e^{i\theta(\mathbf{r})})^2(\Delta_P\Delta_{P'})^*$ is allowed if the local phase gradient matches the canting momentum $p = (P + P')/2$. This leads to a locking term at some distance from the vortex core where the phases are matched. The possible detection of the canting angle will be discussed in the next section.

With the above understanding of PDW-driven scenario, we propose the following phenomenological picture explaining the recent STM experiment in $Bi_2Sr_2CaCu_2O_8$, 17% doping, up to 8.5 T: (1) short-range PDW is pinned by the vortex core and extends to its correlation length.

(2) We estimate the intrinsic correlation length of PDW to be 16 lattice constants. The period-8 CDW appears to have a shorter correlation length ~8 lattice constants as determined from the width of the Fourier transform peak by fitting it to a Gaussian. Part of this width is not intrinsic and is due to the 2π phase winding.

(3) The period-8 CDW produces as a harmonic a period-4 CDW, which we have labeled as CDW_B. Its width is subject to the same blurring as the period-8 CDW. On the other hand, the static PDW near vortex core nucleates the period-4 CDW_A by $\Delta^*_{-Q/2}\Delta_{Q/2}$, which is not affected by the phase winding around the vortex. These two CDWs may have different form factors and different asymmetry factors between x direction and y direction. However, it is hard to extract their correlation length separately based on the current data, since their Fourier peaks mix together. The width of $2\pi/4$ Fourier peak translates to a correlation length around 4a. This serves as a lower bound of the intrinsic correlation lengths of CDW_A and CDW_B.

(4) At zero field, $\Delta_{-Q/2}$ and $\Delta_{Q/2}$ fluctuate with time, we rely on their relative phase being pinned by spatial inhomogeneity to give a static CDW_A. This effect gives much weaker period-4 CDW puddles with a very short correlation length of order 2a. This CDW is unidirectional in each small puddle. We tentatively identify the unidirectional part of CDW both in zero field and in the vortex core as CDW_A.

(5) The static-PDW-enhanced correlation length of CDW_A is enough to give some overlap between neighboring vortices. It is energetically favorable for the unidirectional part to align

its direction and stretch its phase between vortices smoothly to gain overlap energy.

(6) PDW-driven model predicts the absence of $(2\pi/8, 2\pi/8)$ peak. (7) Given the strong pinning effect and relatively small correlation length, these CDWs may not be able to overcome the local pinning effect and become phase coherent between halos.

IV. EXPERIMENTAL PROPOSAL

The disappearance of $(\frac{2\pi}{8}, \frac{2\pi}{8})$ CDW order is surprising for a CDW-driven model while it can be naturally explained in PDW-driven model, as shown in last section. Despite this already existing evidence favoring PDW-driven model, more experimental predictions need to be tested to fully settle down this issue. In this section, we propose experiments to distinguish PDW-driven and CDW-driven scenario unambiguously. Besides, in PDW-driven scenario, our proposed experiment can extract the relative phase between PDW order parameter and d-wave order parameter, which is physical.

The main prediction of PDW-driven scenario is that CDW order parameters at $Q_x/2 = (\frac{2\pi}{8}, 0)$ and $Q_y/2 = (0, \frac{2\pi}{8})$ have the following profile as shown in Eq. (9):

$$\rho_{\mathbf{Q}_a/2}(r,\theta) = e^{i\phi_a} F_P(r) \cos(\theta - \theta_a), \tag{14}$$

where (r,θ) is the polar coordinate of real space around the vortex center and a denotes x or y direction.

$F_P(r)$ vanishes at $r = 0$ and decays as $e^{-\frac{r}{\xi}}$ at large r. It has maximum at nonzero distance to center. $\theta_x = \theta_{P_x} - \theta_d$ and $\theta_y = \theta_{P_y} - \theta_d$ are the relative phases of PDW order parameters $\Delta_{\pm P_a} = |\Delta_{P_a}| e^{i\theta_{P_a} \pm i\phi_a}$ compared to d-wave order parameter $\Delta_D(r,\theta) = |\Delta_D| e^{i\theta_d} e^{i\theta}$

In contrast, a CDW-driven scenario shows a quite distinct profile of period-8 CDW order parameter:

$$\rho_{\mathbf{Q_a}/\mathbf{2}}(r,\theta) = e^{i\phi_a} F_c(r). \tag{15}$$

$F_c(r)$ has maximum at $r = 0$ and decays far away with $e^{-\frac{r}{\xi}}$. The CDW order parameter does not have angle dependence in this scenario.

Clearly, the CDW order parameter profiles from PDW-driven and CDW-driven models have both different radius dependence and angle dependence. A real-space plot of LDoS can be found in Fig. 3. The $\cos(\theta - \theta_a)$ factor in the PDW-driven model means a superposition of strength ± 1 dislocation of CDW order parameter and, in principle, STM experiments can extract θ_a.

Here we will propose the following experimental predictions to distinguish the above two different CDW profiles. In the STM experiment, what is measured is the local density of states (LDoS) at a fixed energy $\nu(\mathbf{r}, E)$. For a fixed energy, $\nu^E(\mathbf{r}) = \nu(\mathbf{r}, E)$ has the same symmetry as density and we expect it to follow Eqs. (14) and (15).

Before going to specific predictions, it may be worthwhile to give one general suggestion to the data analysis procedure of the experimental data. For both PDW-driven and CDW-driven scenarios, the phase of the CDW order with momentum Q_a is expected to be locked to position of the vortex center. As a result, signals from different vortex halos are not coherent. Therefore it is better to shift the position of each vortex center to the origin when doing a Fourier transformation for each vortex halo. In this way, we can make different vortex halos coherent and greatly enhance signals.

The following are predictions for the PDW-driven scenario and how to detect it in experiment. As a benchmark, we show our numerical simulation data. The method of our simulation is summarized in Appendix B. The profile of the d-wave order parameter is $\Delta_D(r,\theta) \sim \frac{r}{\sqrt{r^2+r_0^2}}$ with a vortex core size $r_0 = 3.5$ lattice constants. We used a profile of PDW with r dependence as $\Delta_P(r,\theta) \sim e^{1-\sqrt{r^2+\xi^2}/\xi}$ with correlation length $\xi = 15$. In the following, the local density of states $\nu^E(r)$ is obtained at a fixed energy $E = 30$ meV. Note we only show the d-wave form of bond LDoS because the CDW generated by our model is dominated by the d wave. However, we expect our predictions in the following sections do not rely on form factor.

A. Split peaks for period-8 CDW

The first prediction for the PDW scenario is that the peak at $\mathbf{Q_a}/\mathbf{2}$ is split into two peaks in the direction decided by θ_a. Recall that the density modulation $\rho(\mathbf{r}) = \int_{-\infty}^{0} dE\, \nu^E(\mathbf{r})$ is given by the integral of LDoS $\nu^E(\mathbf{r})$ over the occupied states. We define the slowly varying complex amplitude $\nu^E_{\mathbf{Q_a}/\mathbf{2}}(\mathbf{r})$ by

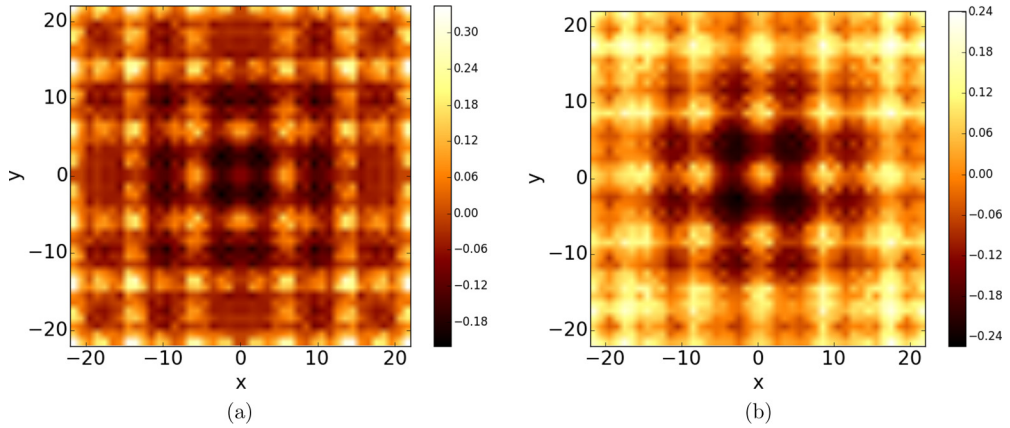

FIG. 3. Real-space plot of on-site LDoS $\nu^E(\mathbf{r})$ at $E = 30$ meV for PDW-driven and CDW-driven models. (a) PDW-driven and (b) CDW-driven models.

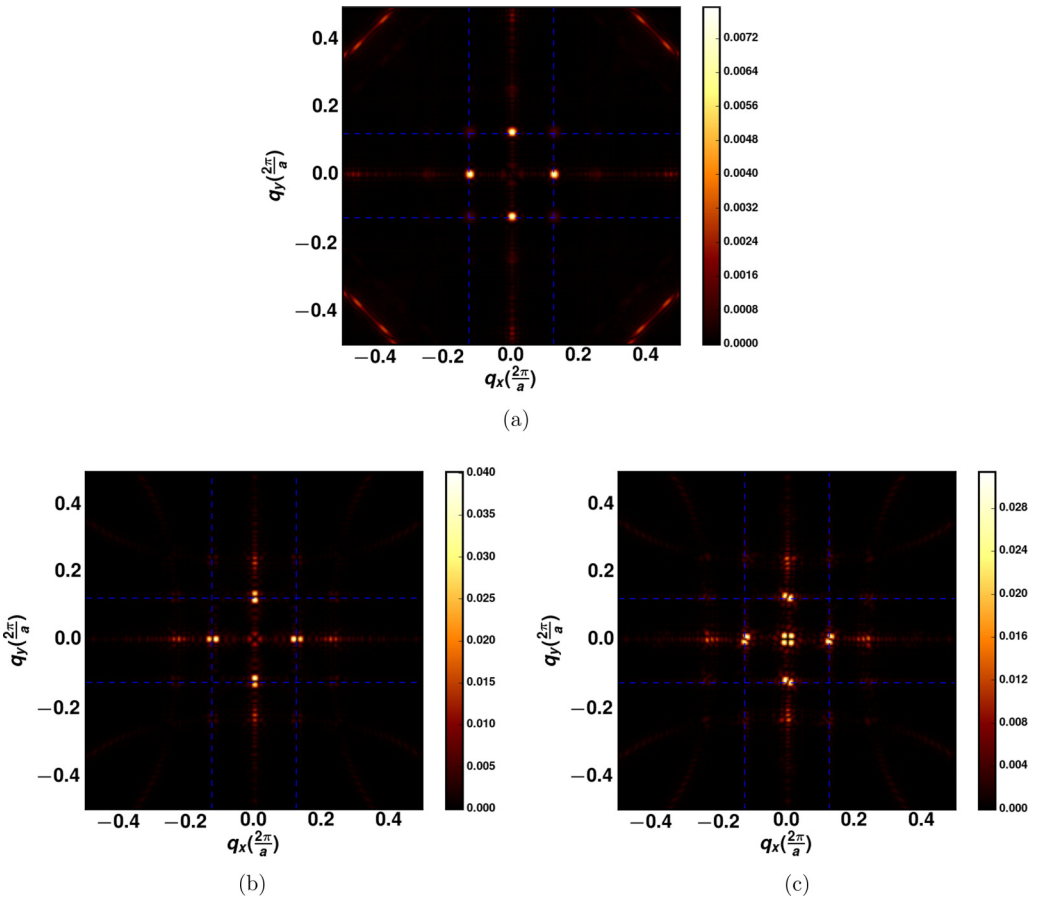

FIG. 4. $|\tilde{\nu}^E(q)|$ with $E = 30$ meV for PDW-driven and CDW-driven models; (a) CDW-driven, (b) PDW-driven: $\theta_x = 0$ and $\theta_y = \frac{\pi}{2}$, (c) PDW-driven: $\theta_x = \frac{\pi}{4}$ and $\theta_y = \frac{3\pi}{4}$.

writing the real-space local DoS as $\nu^E(\mathbf{r}) = \sum_a \nu^E_{\mathbf{Q_a}/2}(\mathbf{r}) e^{\frac{1}{2}i\mathbf{Q_a}\cdot\mathbf{r}} + \text{H.c.}$. This is the analog of $\rho_{\mathbf{Q_a}/2}$ discussed in the last section. We assume that $\nu^E_{\mathbf{Q_a}/2}(\mathbf{r})$ has a similar real-space profile as $\rho_{\mathbf{Q_a}/2}$ as given in Eq. (14), i.e., it is confined to the vicinity of the vortex core and importantly, is proportional to $\cos(\theta - \theta_a)$. Recall that this factor encodes the phase winding of the d-wave superconductor and is therefore an important signature for the PDW-driven scenario..This assumption is supported by our numerical simulations, and will be discussed and shown in greater detail later in Figs. 6 and 7.

We define $\tilde{\nu}^E(\mathbf{q})$ to be the Fourier transform of $\nu^E(\mathbf{r})$. For $\mathbf{q}$ in the vicinity of $\mathbf{Q_a}/\mathbf{2}$, we define

$$\tilde{A}_a(\mathbf{q}) = \tilde{\nu}^E(\mathbf{q} - \mathbf{Q_a}/2) = \sum_{\mathbf{r}} \nu^E_{\mathbf{Q_a}/2}(\mathbf{r}) e^{-i\mathbf{q}\cdot\mathbf{r}}. \tag{16}$$

Consider a in the x direction. When $\theta_a = 0$, it is easy to see that the absolute value of $\tilde{A}_a(\mathbf{q})$ has two peaks in x direction because of the $\cos\theta$ factor. This is because $\cos\theta = \frac{x}{\sqrt{x^2+y^2}}$ produces a line of zero in $\nu^E_{\mathbf{Q_a}/2}(\mathbf{r})$ along the y direction through the vortex core. $\nu^E_{\mathbf{Q_a}/2}(\mathbf{r})$ is odd under $x \to -x$ and as a result $\tilde{A}_a(\mathbf{q_x} = 0) = 0$ and $\tilde{A}_a(\mathbf{q})$ has a splitting along the $\mathbf{q_x}$ direction. The splitting is roughly $\delta q \sim \frac{1}{\xi}$. For general a and general θ_a, the line of zero in $\tilde{A}_a(\mathbf{q})$ is rotated by an angle θ_a. Therefore the absolute value of $\tilde{\nu}^E(\mathbf{q})$ should have two peaks at $\mathbf{q} \approx \mathbf{Q_a}/\mathbf{2}$ with the splitting in the direction of θ_a.

This prediction is confirmed by numerical simulation results for both PDW-driven model and CDW-driven model in Fig. 4. Here we show two different phase choices for the PDW-driven model. The splitting of period-8 peak along the direction θ_a is very clear for PDW-driven models while the CDW-driven model shows one single peak.

Therefore we suggest to fit experimental data with a split-peak model. In our simulation, if we choose the vortex center as the origin, we find that $\tilde{\nu}^E(\mathbf{q})$ is dominated by the real part. Thus it is better to plot only the real part of $\tilde{\nu}^E(\mathbf{q})$. Besides, there should be a sign change at $\mathbf{q} = (\frac{1}{8}\frac{2\pi}{a}, 0)$ if we plot $\text{Re}\nu^E(q_x)$ along $q_y = 0$ cut, as shown in Fig. 5. Again, this comes from the Fourier transformation of $\cos(\theta)$.

B. Direct visualization of "dislocation"

To have a direct visualization of profile shown in Eq. (14) for a PDW-driven model, we need to extract the local CDW order parameter $\nu^E_{\mathbf{Q_a}/2}(x, y)$ from the STM data $\nu^E(x, y)$. For each position (x_0, y_0), we construct a new image by multiplying a Gaussian mask:

$$\bar{\nu}^E(\mathbf{r}; \mathbf{r_0}) = e^{-\frac{|\mathbf{r}-\mathbf{r_0}|^2}{2W^2}} \nu^E(\mathbf{r}). \tag{17}$$

We found that $W = 8$ is a good choice in our simulation. Then we can extract the local CDW order parameter $\nu^E_{\mathbf{Q_a}/2}(\mathbf{r_0})$ by a

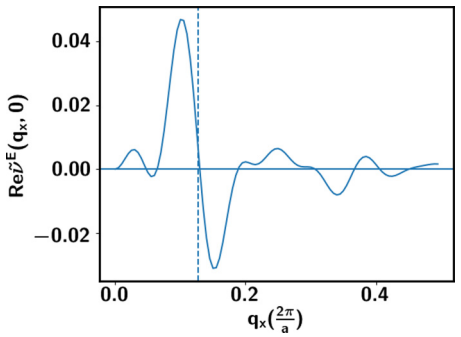

FIG. 5. $\mathrm{Re}\tilde{\nu}^E(q_x,0)$ for PDW-driven model with $\theta_x = 0$ and $\theta_y = \frac{\pi}{2}$; there is a clear sign change at $q_x = \frac{1}{8}\frac{2\pi}{a}$.

Fourier transformation of $\tilde{\nu}^E(\mathbf{r};\mathbf{r_0})$:

$$\nu^E_{\mathbf{Q_a}/2}(\mathbf{r_0}) = \sum_{\mathbf{r}} \tilde{\nu}^E(\mathbf{r};\mathbf{r_0}) e^{-\frac{1}{2}i\mathbf{Q_a}\cdot\mathbf{r}}. \tag{18}$$

After extracting $\nu^E_{\mathbf{Q_a}/2}(\mathbf{r_0})$ for each position, we can easily visualize it and decide whether there is a superposition of strength ± 1 dislocations.

The above algorithm can also be implemented by a filter algorithm in momentum space directly as in Ref. [58]:

$$\nu^E_{\mathbf{Q_a}/2}(\mathbf{r_0}) = \sum_{\mathbf{q}} \tilde{\nu}^E(\mathbf{q}) G(\mathbf{Q_a}/2 - \mathbf{q}) e^{-i(\mathbf{Q_a}/2-\mathbf{q})\cdot\mathbf{r}_0}, \tag{19}$$

where the filter is $G(\mathbf{q}) = \sum_r e^{-\frac{|\mathbf{r}|^2}{2W^2}} e^{-i\mathbf{q}\cdot\mathbf{r}} = e^{-\frac{W^2}{2}|\mathbf{q}|^2}$.

Here we show visualization for simulated data of $|\nu^E_{\mathbf{Q_a}/2}|^2$ from both the CDW-driven and PDW-driven models in Fig. 7. The distinction is very obvious. For a CDW-driven model, $\nu^E_{\mathbf{Q_a}/2}$ has maximal intensity at vortex center. For a PDW-driven model, $|\nu^E_{\mathbf{Q_a}/2}|$ vanishes along a line across the vortex center in the direction of $\theta_a \pm \frac{\pi}{2}$, in agreement with a $\cos(\theta - \theta_a)$ angle dependence. Across the dark line, the phase of local amplitude $\nu^E_{\mathbf{Q_a}/2}$ has a π shift, as shown in Fig. 6(a). We can see the phase of $\nu^E_{\mathbf{Q_a}/2}$ is ϕ_a or $\phi_a + \pi$. Therefore we can remove the overall phase by $\nu^E_{\mathbf{Q_a}/2} \to \nu^E_{\mathbf{Q_a}/2} e^{-i\phi_a}$ and make it real. Then the angle dependence $\nu^E_{\mathbf{Q_a}/2} \sim \cos(\theta - \theta_a)$ can be visualized directly in Fig. 6(c). For unidirectional PDW, Wang *et al.* [49] also noted the phase jump by π by tracking the position of the DOS peaks in real space [49]. In Fig. 6(b), we plot $\mathrm{Re}\nu^E_{\mathbf{Q_x}/2}(x)$ at fixed y. For $y = 0$, $|\nu^E_{\mathbf{Q_x}/2}(x)|$ gives the radius dependence $F(r)$. We can see that the maximum is at finite r. However, our simulation may overestimate the maximum because of boundary effects due to finite size.

Finally, we comment on challenges to apply this algorithm to real experimental data and possible ways to increase the signal to noise ratio. (1) The existence of multiple vortices and impurities modifies the $\cos(\theta - \theta_a)$ angle dependence. In general, there is no time reversal symmetry or any lattice symmetry left, and $\nu^E_{\mathbf{Q_a}/2}(\mathbf{r_0})$ is complex. Thus the line of zero we predicted in the simple model may not be exact. We still expect the real and imaginary parts of $\nu^E_{\mathbf{Q_a}/2}(\mathbf{r_0})$ to each have a line of zero but the lines will no longer coincide. As a result the line of zeros shown in Figs. 7(c)–7(f) will partially fill in. However, in the current experiment [21], the distance between neighboring vortices is roughly three times of the size of the halo; the distortion of the CDW profile by neighboring vortices is not significant. Furthermore, the phase locking mechanism we discussed in the previous section predicts that the Fourier peak of CDW around each vortex splits in the same direction.

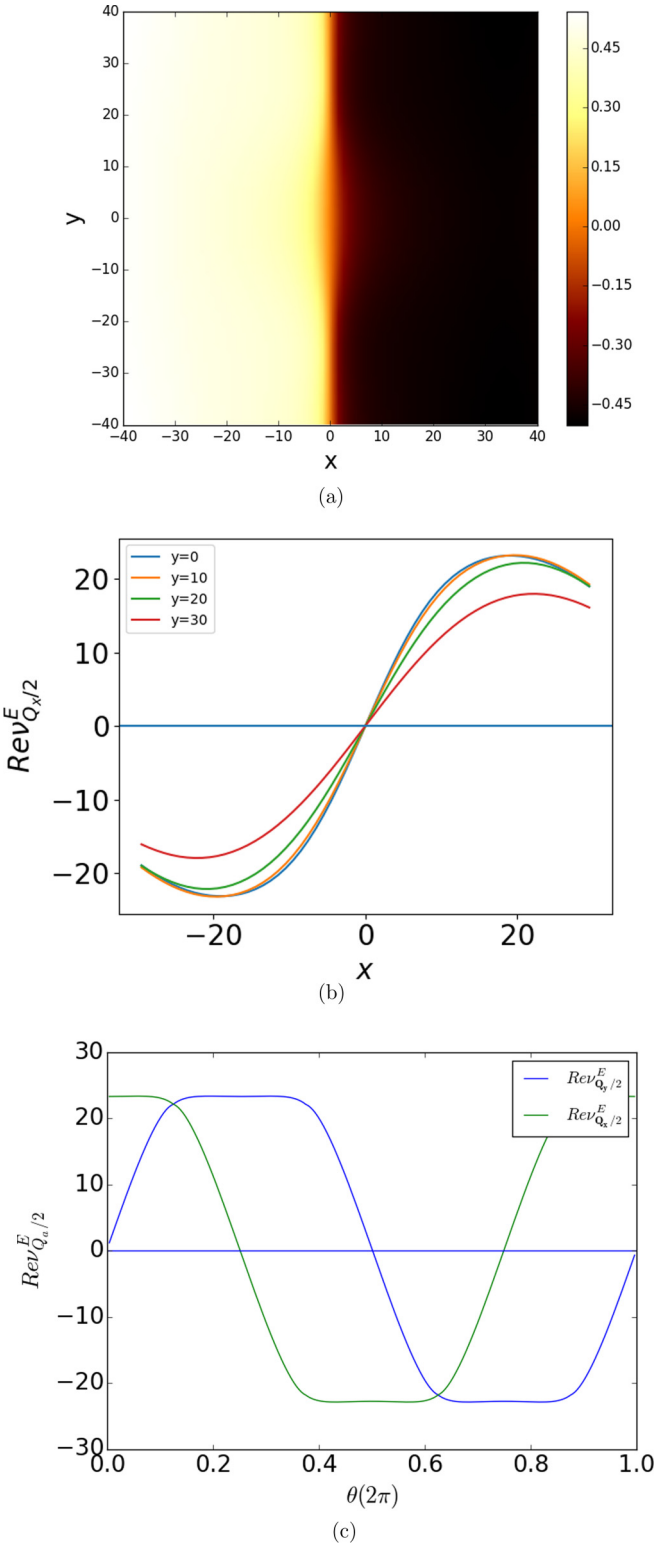

FIG. 6. $\nu^E_{\mathbf{Q_a}/2}$ for PDW-driven model with $\theta_x = 0$ and $\theta_y = \frac{\pi}{2}$. (a) $\arg \nu^E_{\mathbf{Q_x}/2}(x)$. Phase of $\nu^E_{\mathbf{Q_x}/2}(x)$ jumps from $-\pi/2$ to $\pi/2$ across the line $x = 0$. (b) Re $\nu^E_{\mathbf{Q_x}/2}(x)e^{-i\phi_x}$ at fixed y. (c) Re $\nu^E_{\mathbf{Q_a}/2}(\theta)e^{-i\phi_a}$ at $r = 15$. There is a clear cosinelike dependence.

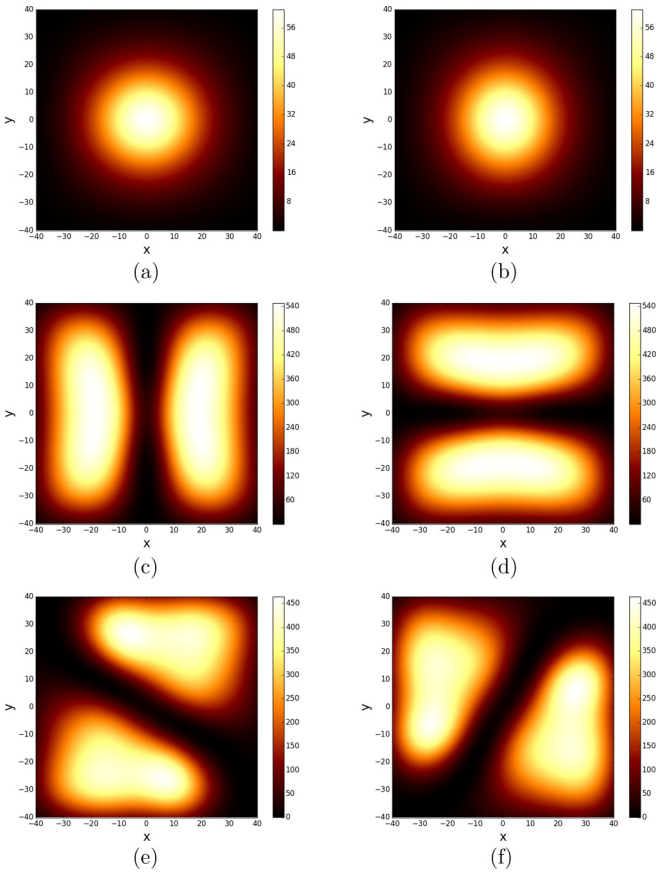

FIG. 7. $|v^E_{\mathbf{Q_a}/2}|^2$ from CDW-driven and PDW-driven models. (a) and (b) are from a CDW-driven model; others are from PDW-driven models. $E = 30$ meV. (a) Local $|v^E_{\mathbf{Q_x}/2}|^2$; CDW-driven model (b) local $|v^E_{\mathbf{Q_y}/2}|^2$; CDW-driven model (c) local $|v^E_{\mathbf{Q_x}/2}|^2$; $\theta_x = 0$ and $\theta_y = \frac{\pi}{2}$; (d) local $|v^E_{\mathbf{Q_y}/2}|^2$; $\theta_x = 0$ and $\theta_y = \frac{\pi}{4}$; (e) local $|v^E_{\mathbf{Q_x}/2}|^2$; $\theta_x = \frac{\pi}{4}$ and $\theta_y = \frac{3\pi}{4}$; (f) local $|v^E_{\mathbf{Q_y}/2}|^2$; $\theta_x = \frac{\pi}{4}$ and $\theta_y = \frac{3\pi}{4}$.

Thus the split peak signal should be observable in the existence of multiple vortices. (2) There is a smooth background, which will add an offset to the $\cos(\theta - \theta_a)$ factor. If we assume the background is smooth, it can be subtracted with a sophisticated data analysis technique. (3) Although it is not necessary to analyze each vortex separately, doing it may increase the signal to noise ratio. If we choose the origin of Fourier transformation to be the center of each vortex, our PDW-driven model predicts the Fourier amplitude of the period-8 CDW to be real. We expect the noise to have a random phase, and plotting the real part of the amplitude instead of the absolute value can enhance the signal to noise ratio.

C. Flux density wave

In the PDW-driven scenario, we will also get a flux density wave. The orbital magnetic moment of each plaquette $M(\mathbf{r})$ can be estimated through the following equation:

$$M\left(\mathbf{r}+\frac{\hat{x}}{2}+\frac{\hat{y}}{2}\right) = \frac{a^2}{4}(I(\mathbf{r},\mathbf{r}+\hat{\mathbf{x}}) + I(\mathbf{r}+\hat{\mathbf{x}},\mathbf{r}+\hat{\mathbf{x}}+\hat{\mathbf{y}}) + I(\mathbf{r}+\hat{\mathbf{x}}+\hat{\mathbf{y}},\mathbf{r}+\hat{\mathbf{y}}) + I(\mathbf{r}+\hat{\mathbf{y}},\mathbf{r})), \tag{20}$$

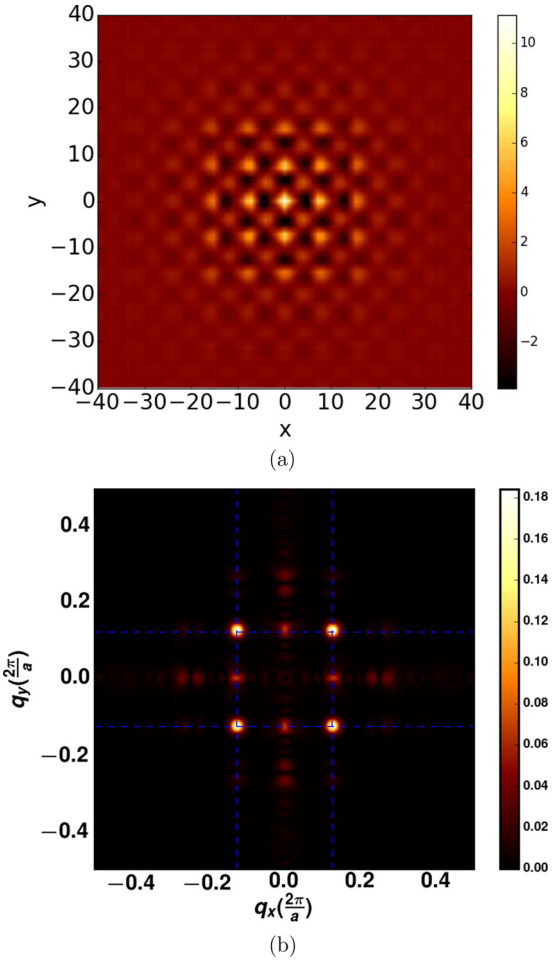

FIG. 8. Flux density wave pattern from the PDW-driven model in vortex halo. (a) Real-space pattern of magnetic moment $M(\mathbf{r})$ in units of $10^{-3}\mu_B$. (b) Magnetic moment $M(q)$ in momentum space.

where $a = 3.5$ Å is the lattice constant. $I(\mathbf{r},\mathbf{r}+\hat{\mathbf{r}}_\mathbf{a})$ is the current going through the bond from $\mathbf{r}$ to $\mathbf{r}+\hat{\mathbf{r}}_\mathbf{a}$, where a denotes x or y.

$M(\mathbf{r})$ has a density wave with momentum $\mathbf{Q_x}/2 = (\frac{2\pi}{8},0)$, $\mathbf{Q_y}/2 = (0,\frac{2\pi}{8})$. There is also a density wave in the diagonal direction $Q_{\pm,\pm} = (\pm\frac{2\pi}{8}, \pm\frac{2\pi}{8})$. The real space and momentum space patterns of magnetic moment are shown in Fig. 8. The amplitude of the density wave at momentum $(\frac{2\pi}{8},\frac{2\pi}{8})$ is around $0.005\mu_B$ and may be possible to be detected by a neutron scattering experiment. The observation of a flux density wave at this wave vector offers the opportunity to definitively settle the question of unidirectional versus bidirectional PDW.

D. Other types of PDW

This paper is mainly focused on the bidirectional PDW model. However, other types of PDW state have been proposed before. In this section, we show signatures for unidirectional PDW and canted PDW models. Therefore STM experiments can rule out or support these kinds of PDW models.

For the unidirectional PDW shown in Fig. 9 with only an x component, the Fourier transform data only show a peak at

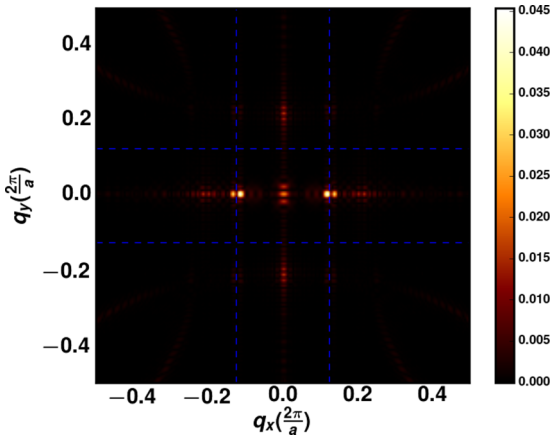

FIG. 9. $|\tilde{\nu}^E(q)|$ for a unidirectional PDW with phase $\theta_x = 0$.

$\mathbf{Q_x/2}$, not at $\mathbf{Q_y/2}$. There is still a split peak consistent with our previous discussions for bidirectional PDW.

For canted PDW, we expect the peak in $\nu^E(q)$ deviates from (1,0) and (0,1) directions. For the canted PDW model with shifted momentum $p = 0.03 * 2\pi/a$, $\mathbf{P_1} = (\frac{2\pi}{8}, p)$, $\mathbf{P_1'} = (-\frac{2\pi}{8}, p)$ and $\mathbf{P_2} = (p, \frac{2\pi}{8})$, $\mathbf{P_2'} = (p, -\frac{2\pi}{8})$ this shift shows up in Fig. 10. Because of condition $\tilde{\nu}^E(q) = \tilde{\nu}^E(-q)^*$, we see double peak with shift p. In experiment it may be better to detect this feature with complex amplitude $\tilde{\nu}^E(q)$ instead of intensity $|\tilde{\nu}^E(q)|$.

If we can decide the value of shift momentum $|p|$ from Fourier transformation data, then we can extract a local order parameter $\nu_P^E(\mathbf{r})$ with $P_\pm = (\frac{2\pi}{8}, \pm p)$ following Eq. (17). It turns out that $P = (\frac{2\pi}{8}, p)$ has an antivortex while $P = (\frac{2\pi}{8}, -p)$ has a vortex, as shown in Fig. 11.

If momentum resolution is not good enough to decide the value of p, we propose to visualize $\nu_{P_0}^E((r))$ with $P_0 = (\frac{2\pi}{8}, 0)$. If it is ordinary PDW-driven, we get a similar plot as in Fig. 6(a). If it is canted PDW-driven, we will get a strange position dependence of arg $\nu_{P_0}^E(\mathbf{r})$ like in Fig. 12(b). This is a signature of canted PDW and it is consistent with the following equation:

$$\nu_{P_0}^E(\mathbf{r}) \sim \cos(\theta - py). \tag{21}$$

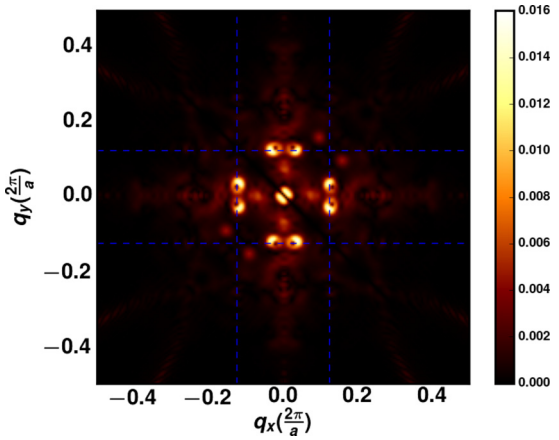

FIG. 10. $|\tilde{\nu}^E(\mathbf{q})|$ for a canted PDW with shifted momentum $p = 0.03 \times 2\pi/a$. The phase of PDW is $\theta_x = 0$ and $\theta_y = \frac{\pi}{2}$.

V. SUMMARY

We now summarize some of the conclusions from the discussion in previous sections. The observation of period-8a bidirectional charge order in the vortex halo directly means that there are induced order parameters $\rho_{Q_x/2}, \rho_{Q_y/2}$. In the presence also of a nonzero superconducting order parameter Δ_d of the usual d-wave superconductor, the period-8 charge order necessarily implies that there are also period-8 modulations in the superconducting order parameter $\Delta_{Q_x/2}, \Delta_{Q_y/2}$, i.e., pair-density wave order at the same period. Given this obvious equivalence in the superconductor between charge and pairing modulations, it may seem to be a moot question whether what is observed is primarily charge order or pair order at period 8. Nevertheless, we have shown that there are two distinct possibilities for the observed period-8 order which naturally correspond to two distinct driving mechanisms.

In the CDW-driven scenario, we simply postulate that there are slow fluctuations of a previously unidentified period-8 CDW in the uniform superconductor. In the vicinity of the vortex, the breaking of translational symmetry and the weakening of the superconducting order may then pin the fluctuations of the period-8 CDW and lead to static ordering. Period-4 charge order then appears as a subsidiary order. In this scenario, it is natural to expect that the phase of the induced CDW order does not wind on going around the vortex core.

In the PDW-driven scenario, on the other hand, we postulate that there are slow fluctuations of period-8 PDW that are pinned in the vortex halo. The induced period-8 CDW then will have a strength ± 1 dislocation centered at the vortex core. More precisely, the induced period-8 CDW will be a superposition of a configuration with a strength $+1$ dislocation and one with a strength -1 dislocation. This leads to a rather different spatial profile for the induced period-8 CDW. A further difference is that there are now two distinct kinds of induced period-4 CDW orders which we have referred to as CDW_A and CDW_B. The CDW_A pattern has no winding around the vortex core, while the CDW_B pattern is a superposition of strengths-± 2 dislocations.

We discussed the extent to which existing data support either scenario. In particular, in the PDW-driven scenario, there is a natural explanation for the absence of peaks at $2\pi(\frac{1}{8}, \frac{1}{8})$ as reported in the experiments. It is, however, important to analyze the data more carefully to clearly establish which of these scenarios is realized, and we described a number of distinguishing features. Most importantly, the spatial profile of the induced charge orders due to the dislocation structure in the PDW-driven scenario should be discernible using the methods we describe.

Note that within either of these scenarios there is no general reason for a predominantly d-form factor period-8 charge order to induce only an s-form factor period-4 charge order [50]. From our numerical simulation of d-wave PDW coexistence with a uniform d-wave superconductor, the period-8 CDW we get is actually dominated by d wave, instead of s-wave form factor from the naive expectation. Thus we do not have a natural explanation of the observations on form factors in the experiments.

A further question that one can ask is whether the fluctuation order that is pinned on the halo is unidirectional or

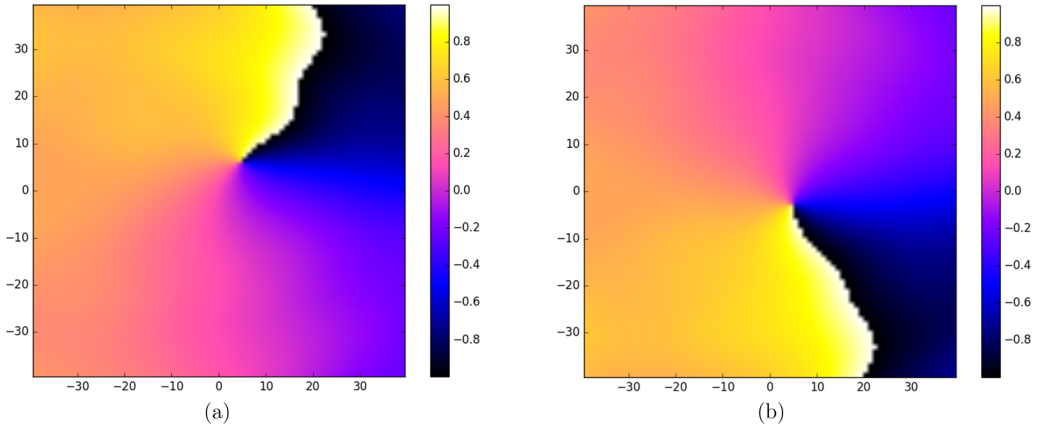

FIG. 11. $\arg \nu_P^E(\mathbf{r})$ for canted PDW in units of π. (a) $P = (\frac{2\pi}{8}, p)$. (b) $P = (\frac{2\pi}{8}, -p)$.

bidirectional. The observed period-8 modulations are apparently bidirectional. The simplest explanation therefore is that the "parent" order is also bidirectional. However, one may postulate that there are domains of different unidirectional patches within the vortex halo. This may be easy to check in the STM data.

Finally, an important question is whether the period-8 PDW (if it is really the driver) is merely a competing/intertwined order with the standard d-wave superconductor or whether it is a "mother" state with a very large amplitude that controls the physics up to a much larger energy scale than the standard d-wave order itself. Just based on the STM experiments alone there does not seem to be any clear way to answer this question. However, in the following section, by combining with information from other existing experiments, we will provide suggestive arguments in favor of a mother PDW state.

VI. A BROADER PERSPECTIVE ON PDW AND ITS RELATION TO THE PSEUDOGAP STATE OF THE CUPRATES

In this section, we take a broader perspective and ask whether the message learned from the STM data on Bi-2212 can inform us on anomalies observed in other cuprates and more generally on the pseudogap itself. We shall assume that the data are described by the fluctuating PDW ("mother state") scenario and we shall assume that the scenario continues to hold in other underdoped cuprates. We focus our attention on YBCO where extensive data on the CDW up to high magnetic field are available [17–19]. The picture that emerges from these studies is that SRO CDW appears below about 150 K over a doping range between $x = 0.09$ and 0.16 [12]. This SRO CDW has very weak interlayer ordering centered around $L = 1/2$, where L is the c-axis wave vector in reciprocal lattice unit. These peaks grow with decreasing temperature but their strength weakens and their in-plane linewidth broadens below T_c. These peaks occur along both a and b axes. Above a field of 15 to 20 T, a unidirectional CDW emerges and rapidly becomes long range along the b axis. The onset of long-range ordered CDW is consistent with earlier NMR data [16,59]. At the same time, the SRO CDW remains along both a and b axes. Thus the high magnetic field data show that there are two kinds of CDW with the same incommensurate period which does not change with magnetic field. As the experimentalists remarked [18,19], this is very puzzling because having the same incommensurate wave vector suggests the two kinds of CDW share a common origin.

If we interpret the observed CDW as subsidiary to a fluctuating PDW, the latter must exist above the CDW onset at 150 K and most likely above T^* which is taken as the thermodynamic

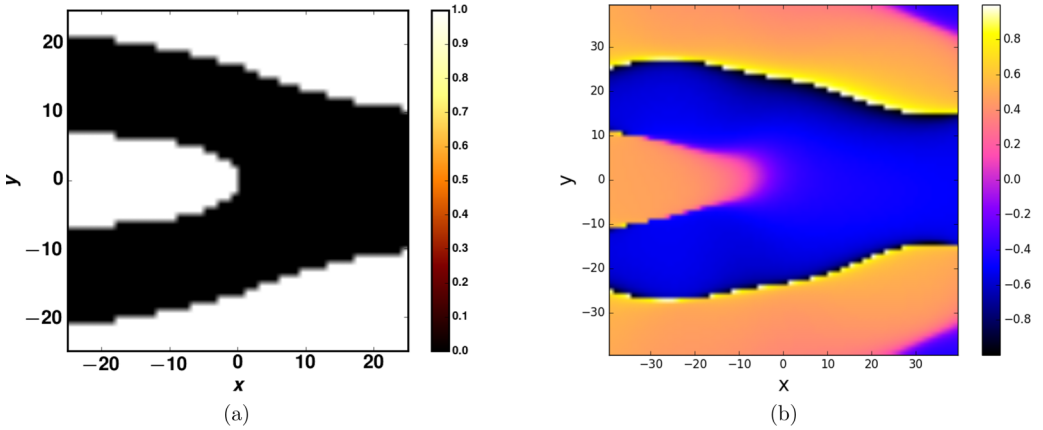

FIG. 12. Visualization of $\arg \nu_{P_0}^E(\mathbf{r})$ for canted PDW-driven model. $P_0 = (\frac{2\pi}{8}, 0)$ and shifted-momentum is $p = 0.03 \times 2\pi$. (a) $\arg \cos(\theta - py)$ in Eq. (21). (b) $\arg \nu_{P_0}^E(\mathbf{r})$ from the canted PDW-driven model.

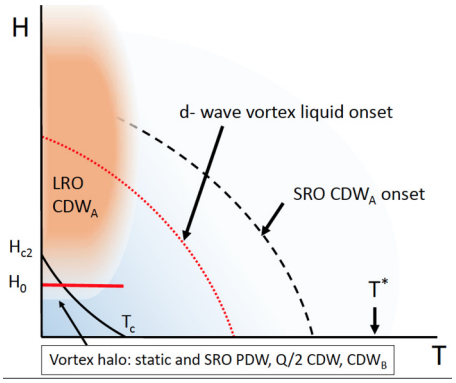

FIG. 13. H-T Phase diagram for an underdoped cuprate. The light blue shading indicates that a fluctuating PDW is pervasive over a large segment of the H-T plane for underdoped cuprates. Dashed line indicates the onset of short-range ordered CDW at wave vector Q. It is a subsidiary order of the PDW, which we refer to as CDW$_A$. Solid red line marks the magnetic field H_0 as defined in Eq. (14) in terms of the coherence length ξ_P of the PDW, which marks the size of the vortex halo. It is closely related to the field H_{c2}, which marks the onset of a vortex solid phase and LRO superconductivity. Within this phase and inside the vortex halo, we expect the pinned static PDW, $Q/2$ CDW as well as its harmonic, a wave-vector Q CDW, which we refer to as CDW$_B$. The CDW$_B$ short-range order state may extend to a higher magnetic field much beyond H_{c2}. The dotted red line indicates the onset of a vortex liquid phase. The brown area indicates the appearance of long-range ordered type-A CDW with wave vector Q.

signature of the pseudogap. Similarly, we take the viewpoint that quantum oscillations require the existence of bidirectional CDW [60], which implies that fluctuating PDW extends to magnetic fields of 100 T and beyond. By continuity, we expect fluctuating PDW to cover a large segment of the H-T plane, as shown in Fig. 13. The PDW must be strongly fluctuating in time, because there is no sign of superconductivity from transport measurements outside of a limited region near T_c and H$_{c2}$. However, diamagnetic signals are observed over a much larger regime [43], a point which we shall return to later. Nevertheless, our picture is that the subsidiary orders such as CDW can be more robust and make their presence felt. This is particularly true of CDW$_A$ (see Eq. 10), which does not require d-wave pairing for its presence. So we assign CDW$_A$ to be the SRO CDW that onsets below 150 K, as shown by the dashed line in Fig. 13.

Below T_c the phase stiffness of the LRO d-wave robs oscillator strength from the PDW, diminishing its already weak phase stiffness even further. This explains the reduction of the CDW strength below T_c. On the other hand, we saw in Sec. III that in a magnetic field a vortex can pin the PDW to form a static but short range halo around the core. This in turn induces CDW at wave vector $Q/2$ and its harmonic CDW$_B$. All these states are located roughly inside the superconducting region as indicated in Fig. 13. Of course being tied to the vortices means that the strengths of these states are proportional to the magnetic field. Note that we expect the d-wave phase stiffness to be reduced inside the halo while that of the PDW to be strengthened.

We define the field H_0 as

$$H_0 = \phi_0/\left(2\pi\xi_P^2\right), \tag{22}$$

where $\phi_0 = hc/2e$ is the flux quanta in a superconductor, ξ_P is the correlation length of the pinned PDW. The 2π in the denominator has been inserted to make this equation resemble the definition of H_{c2} and the exact numerical factor should not be taken seriously. The point is to provide a scale for the field where the pinned PDW starts to strongly overlap. For $H > H_0$, the d-wave superconductor is being squeezed out and the PDW phase regains its stiffness. It eventually becomes depinned as the d-wave pairing diminishes and resumes its dynamical fluctuation. In this region, the CDW$_A$ grows in strength and coherence, recovering the growth with decreasing temperature that was interrupted by the onset of T_c for $H < H_0$. The fact that the LRO CDW is unidirectional even though the PDW is bidirectional can be rationalized by the following argument. There is a term in the Landau free energy $\gamma_{a,b}|\rho_{Q_x}|^2|\rho_{Q_y}|^2$, where $a,b = x,y$ labels the Cu-O bond in x and y directions. As we discussed previously, the local s-wave and d-wave form factors related to these two bonds do not have symmetry distinction, but there are still two degrees of freedom in each unit cell, and they may behave differently. In the channel where γ is large and positive, the free energy strongly prefers unidirectional order; in the channel where γ is small, we can have bidirectional CDW. In YBCO, the presence of the chain already broke tetragonal symmetry to begin with, making it even more plausible that the order grow strongly in one direction. On the other hand, the term $\Delta_P\Delta^*_{-P}\rho_Q$ is linear in ρ_Q, meaning that some SRO is likely generated in the orthogonal direction. We shall return to this point later.

Returning to the region below H$_{c2}$ we expect to find the pinned PDW and the CDW with period $Q/2$ as static but short-range ordered. This is because the static order of $Q/2$ CDW requires the static order of d-wave pairing as well as PDW. The $Q/2$ CDW should persist to lower field with decreasing amplitude. It may be expected to have correlation length similar to that found in the STM experiment, which we estimate to be about 16 lattice spacings. It will of course be of great interest to search for this by x-ray scattering. On the other hand, the period-Q CDW$_B$ can be thought of as a harmonic of the period-$Q/2$ CDW, but it can exist even in its absence. Thus we expect it to exist up to higher field. We do not know exactly how high a field it can persist to, but it cannot go above the d-wave vortex liquid regime. It is worth noting that in practice there can be remnants of static pinned vortices even above H_c2. Yu *et al.* [43] reported hysteretic behavior which extends to very high field at low temperatures, leading them to identify a second vortex solid regime. The existence of some form of bidirectional CDW that persists up to high field at low temperature is important in order to explain the quantum oscillations. We believe the LRO unidirectional CDW cannot by itself give rise to quantum oscillations, but the combination with some SRO CDW in the direction perpendicular to it may be sufficient. This can come from the bidirectional CDW$_B$ discussed above if it persists to high field, or it is possible that a short-range order CDW$_A$ is generated along direction a at higher field as explained earlier.

In support of the picture outlined above, we note that there are extensive NMR data showing that H$_0$ is typically

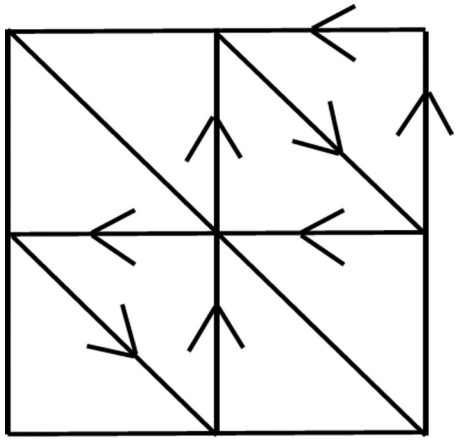

FIG. 14. Illustration of the loop current produced by the canted PDW.

5 to 10 T below the H_{c2} as measured by transport [15,16]. Thus there is a close relationship between H_{c2} and the vortex halo size as defined by the size of the pinned PDW. We also recall that the CDW that we identify as type A in Bi-2212 is unidirectional, which agrees with this assignment for YBCO. We note that the Bi-2212 sample used has a doping of 0.17, which lies on the upper end of the observability of CDW in YBCO samples. The H_{c2} and corresponding H_0 are expected to be very high. So the 8.25 T used in the STM experiment is expected to be far below the regime where CDW_A can achieve long-range order.

In Fig. 13, we add the line H_0 to a phase diagram in the H-T plane for underdoped cuprates, following the proposal of Yu *et al.* [43]. The resistive H_{c2} is the boundary of the vortex solid and marks the resistive transition. (To avoid cluttering, we did not show the emergence of a second vortex solid regime mentioned earlier that extends to high field at low temperature [43].) The key point made by Yu *et al.* is that there is a large region of vortex liquid in the phase diagram where there is strong superconducting amplitude. The evidence for this is a strong diamagnetic signal. Given the small size of the true vortex core where the d-wave coherence peak is destroyed, it is reasonable to interpret the vortex liquid as a region of strong d-wave superconducting amplitude with dynamical vortices that persist to very high field. It is less certain how high in temperature the d-wave vortex liquid extends. It is possible that the diamagnetic signal may come from PDW fluctuations at high fields [35,43]. Thus the location of the dotted line in Fig. 13 that indicates the extent of d-wave vortex liquid is quite uncertain, especially in the temperature direction.

We should mention that similar CDW has been seen in the Hg-based compound. Here the doping range extends further down to x of order 0.06 and up to about 0.12. Another difference is that there is no clear suppression of the CDW at T_c. Instead, its strength seems to saturate. It should be noted that unlike YBCO, this is a tetragonal system. From existing X-ray data, it is not known whether the CDW is bidirectional or unidirectional. Apart from these differences, the observations seem to fit into the same phase diagram shown in Fig. 13.

Finally, we comment on the symmetry breaking observed at the T^* lines, which lies at a temperature above the onset of SRO CDW. This seems to be associated with breaking a lattice symmetry, perhaps a kind of nematic order. Importantly, a recent experiment on the anisotropy of the spin susceptibility [5] found the nematic axis to be along the diagonal in a single layered Hg-based compound, while it is along the bond direction in YBCO [4]. This would rule out nematicity based on CDW, which should be along the bond direction in a single layer tetragonal system. The observation in YBCO can be understood from the stacking of two orthogonal directions of diagonal nematicity in each layer. Such nematicity agrees with the symmetry of the orbital current model [61]. As mentioned earlier, in the PDW model, it was pointed out by Agterberg *et al.* [47] that adding canting to the PDW model as described earlier has the same symmetry as the orbital current model. The four different combinations of $(p1, p2)$ give rise to a four-state clock model. Fluctuations between (1,1) and $(-1, -1)$ restores time reversal symmetry but gives rise to a diagonal breaking of nematic symmetry, just like the orbital current model. Indeed, a canted PDW model will carry intracell currents as shown in Fig. 14, which is the closest we can get to Varma's model in a single band model. As seen in this figure, the current can be understood as supercurrent running along x and y, with a return current along one of the diagonal bond. In fact, we find that such a current pattern emerges from the PDW model. Without self-consistent determination of the mean-field ground state, there is a net current along x and y, which presumably will be fixed by a proper return current in a self-consistent mean-field theory. However, the current we find is very small, on the order of $10^{-3}t$ on each bond. This gives rise to a moment of about $10^{-3}\mu_B$, which is too small compared with the 0.1 μ_B reported by neutron scattering. We note on general ground that the orbital current in the PDW model must be small. Let us define the canted component of the wave vector as $p = (P + P')/2$. The supercurrent can be estimated from the product of the phase gradient which is p and the spectral weight, which is x/m, where $1/m$ is proportional to ta^2. Thus we expect the maximal supercurrent to be $x|p|t$, where p is in reciprocal lattice units. Since $|p|$ should be less than $|P|$, we expect $x|P|$ to be less than 10^{-2} and similarly for the moment in units of μ_B. Thus it is unlikely that the canted PDW model can account for the orbital current observed by neutron. However, it potentially can explain the onset of diagonal nematicity at T^*.

Finally, we call attention to the most interesting part of the phase diagram, the region at zero temperature and above H_{c2}. In our picture this is a ground state consisting of a PDW which does not order due to quantum fluctuations. This state is metallic with some combination of long-range and short-range CDW order, sufficient to form pockets visible by quantum oscillations. What is the nature of this state? Is it a Fermi liquid? Is the dissipation due to the metallic state responsible for quantum disordering the PDW? These are fascinating questions that are beyond the purview of the present phenomenology oriented paper.

VII. CONCLUSION

Based on our analysis, we come to the following conclusions. (1) It is likely that the 8a CDW observed in the STM experiment has its origin in a period-8 PDW, which is pinned to be static near the vortex core. The main evidence based on the currently available data is the absence of a peak at (1/8,1/8),

which would be expected if the 8a-CDW were primary. We propose further analyses of the data which can nail down this conclusion. The main point is that the winding of the d-wave superconducting phase around the vortex core imprints a very special signature on the period-8 CDW, which is visible either as a splitting of the Fourier transform peak or a sign change across an oriented line in the Fourier filtered data.

(2) We think it is likely that the PDW pinned near the vortex core is bidirectional, because both the 8a and 4a CDW observed there appear to be bidiagonal. A bidiagonal PDW can generate unidirectional CDW but the converse is not true: a unidirectional PDW may be able to generate checkerboard patterns made up of patches of unidirectional stripe CDW, but that distinction should be amenable to experimental test.

(3) The naive expectation that the subsidiary 4a order has local s symmetry is not generally correct, given the definition of the form factor used in the STM experiments [50]. In fact, in our microscopic mean-field model, we find these to have mainly d symmetry. The local symmetry depends on the microscopic detail and it is no surprise that it is not captured by our simple mean-field theory, but we want to convey the message that a d symmetry subsidiary order can readily be generated. Thus the observed d-symmetry CDW that is already present at zero field may also be a subsidiary order due to PDW. For Bi-2201, the CDW is close to commensurate with period 4 and we cannot rule out that this CDW is not simply an independent order, as advocated in a recent preprint [49]. On the other hand, the idea of independent order is difficult to justify for YBCO, where two different CDW seem to coexist with the same incommensurate period. We discuss a scenario where both CDW's are subsidiary to the same PDW.

(4) Up to now, the notion of a halo around a vortex core is not a well-defined one. The coherence peak associated with d-wave superconductivity is killed only inside the true core, which has a radius of two or three lattice spacings. The coherence peak remains visible throughout the halo region, indicating that d-wave order is not fully destroyed. We propose that the size of the pinned PDW provides a way to define the halo radius and we introduce a magnetic field scale H_0 associated with this length scale. We relate this field scale to the growth of the 4a CDW observed in underdoped YBCO samples and with H_{c2}.

(5) A canted PDW is an attractive scenario that can unify the pseudophenomenology with the nematic transition observed at T^*. The STM data offer a way to search for this kind of order, even though the required resolution may be challenging.

In summary, we answer the question we first posed in Introduction: we think that that the observed period-8 CDW is opening a new window into the world of underdoped cuprates and pseudogap physics. Much exciting further developments are sure to come.

ACKNOWLEDGMENTS

We thank J. C. Davis and M. Hamidian for sharing with us their data prior to publication and for very helpful discussions. PAL acknowledges the support of NSF under DMR-1522575. T.S. is supported by a US Department of Energy grant DE-SC0008739, and in part by a Simons Investigator award from the Simons Foundation. We thank the Moore Foundation EPiQS program for facilitating our interaction with J. C. Davis. T.S. thanks the conference on High Temperature Superconductivity at the Aspen Center for Physics, which is supported by NSF grant PHY-1607611, for enabling a part of this work.

Z.D. and Y.-H.Z. contributed equally to this work.

APPENDIX A: NUMERICAL CALCULATION OF BAND STRUCTURE OF PDW STATE

For a uniform PDW state, we calculate the band structure by diagonalizing a BdG Hamiltonian $H(k)$ for each momentum k. At each k, we need to use a $81 * 2 = 162$ basis: $\Psi_k = (\psi_\uparrow(k), \psi_\downarrow^\dagger(-k))$. $\psi_\sigma(k)$ is a collection of $9 \times 9 = 81$ electron annihilation operators: $c_{k'}$ with momenta $k' = k + m\mathbf{P_x} + n\mathbf{P_y}$, where $\mathbf{P_x} \approx (\frac{2\pi}{8},0)$ and $\mathbf{P_y} \approx (0,\frac{2\pi}{8})$, $m,n = -4,-3,-2,-1,0,1,2,3,4$. In Sec. III A, we use $\mathbf{P_x} \approx (0.14 \times (2\pi),0)$ and $\mathbf{P_x} \approx (0,0.14 \times (2\pi))$. We set a large truncation for m and n to better capture the effect of subsidiary CDW generated by PDW. In this basis, we rewrite the mean-field Hamiltonian in Eq. (1) at momentum k as

$$
\begin{aligned}
H_k = &\sum_{m,n} \epsilon_{k+m\mathbf{P_x}+n\mathbf{P_y}} c^\dagger_{k+m\mathbf{P_x}+n\mathbf{P_y},\uparrow} c_{k+m\mathbf{P_x}+n\mathbf{P_y},\uparrow} - \sum_{m,n} \epsilon_{-k-m\mathbf{P_x}-n\mathbf{P_y}} c_{-k-m\mathbf{P_x}-n\mathbf{P_y},\downarrow} c^\dagger_{-k-m\mathbf{P_x}-n\mathbf{P_y},\downarrow} \\
&+ \sum_{m,n} 2\Delta(\cos(k_x + mP_x + nP_y - P_x/2) - \cos(k_y + mP_x + nP_y)) c_{k+m\mathbf{P_x}+n\mathbf{P_y},\uparrow} c_{-k-m\mathbf{P_x}-n\mathbf{P_y}+\mathbf{P_x},\downarrow} \\
&+ \sum_{m,n} 2\Delta(\cos(k_x + mP_x + nP_y + P_x/2) - \cos(k_y + mP_x + nP_y)) c_{k+m\mathbf{P_x}+n\mathbf{P_y},\uparrow} c_{-k-m\mathbf{P_x}-n\mathbf{P_y}-\mathbf{P_x},\downarrow} \\
&+ \sum_{m,n} 2\Delta(\cos(k_x + mP_x + nP_y) - \cos(k_y + mP_x + nP_y - P_y/2)) c_{k+m\mathbf{P_x}+n\mathbf{P_y},\uparrow} c_{-k-m\mathbf{P_x}-n\mathbf{P_y}+\mathbf{P_y},\downarrow} \\
&+ \sum_{m,n} 2\Delta(\cos(k_x + mP_x + nP_y) - \cos(k_y + mP_x + nP_y + P_y/2)) c_{k+m\mathbf{P_x}+n\mathbf{P_y},\uparrow} c_{-k-m\mathbf{P_x}-n\mathbf{P_y}-\mathbf{P_y},\downarrow} + \text{H.c.},
\end{aligned}
\tag{A1}
$$

where $\Delta = 45$ meV. For the bare band dispersion ϵ_k, we use a tight-banding model on square lattice with nearest-neighbor hopping $t = 0.21$ eV, second neighbor hopping $t_p = -0.047$ eV, third neighbor hopping $t_{pp} = 0.04$ eV, and fourth neighbor

hopping $t_{ppp} = -0.01$ eV:

$$\epsilon_k = -2t(\cos(k_x) + \cos(k_y)) - 4t_p \cos(k_x)\cos(k_y) - 2t_{pp}(\cos(2k_x) + \cos(2k_y)) \\ -4t_{ppp}(\cos(2k_x)\cos(k_y) + \cos(k_x)\cos(2k_y)) - \epsilon_0. \tag{A2}$$

We fix the chemical potential ϵ_0 self-consistently to match the hole doping.

APPENDIX B: NUMERICAL SIMULATION OF *d*-WAVE VORTEX HALO

We did exact diagonalization to simulate the local density of states (LDoS) inside the vortex halo. Our Hamiltonian for the PDW-driven model is

$$H_P = H_0 + \sum_{\mathbf{x},\mu} F_d(\mu)\left\{|\Delta_D| e^{i\theta_d + i\theta} + \left[\sum_a |\Delta_{P_a}| e^{i\theta_a + i\theta_d} \sin\left(\frac{1}{2}\mathbf{Q_a}\cdot\left(\mathbf{x} + \frac{\mu}{2}\right)\right)\right]\right\} c^\dagger_\uparrow(\mathbf{x}) c^\dagger_\downarrow(\mathbf{x}+\mu) + \text{H.c.}, \tag{B1}$$

where $\mu = \hat{x}$ or $\hat{y}$ labels two different kinds of nearest-neighbor bonds, $F_d(\hat{x}) = 1$ and $F_d(\hat{y}) = -1$, and a stands for x or y. We used $|\Delta_{P_x}| = |\Delta_{P_y}| = 30$ meV at the vortex center in our calculation, away from the vortex center, the PDW profile is

$$\Delta_P(r) = 30 e^{1-\sqrt{r^2+\xi^2}/\xi} \text{ meV} \tag{B2}$$

with $\xi = 15$.

Our Hamiltonian for the CDW-driven model is

$$H_C = H_0 + \sum_{\mathbf{x},\mu} F_d(\mu)|\Delta_D| e^{i\theta_d + i\theta} c^\dagger_\uparrow(\mathbf{x}) c^\dagger_\downarrow(\mathbf{x}+\mu) + \sum_{\mathbf{x},\mu} F_s(\mu)\left[\sum_a |\Delta_{C_a}| e^{i\theta_a} \sin\left(\frac{1}{2}\mathbf{Q_a}\cdot\left(\mathbf{x} + \frac{\mu}{2}\right)\right)\right] \sum_\sigma c^\dagger_\sigma(\mathbf{x}) c_\sigma(\mathbf{x}+\mu) + \text{H.c.}, \tag{B3}$$

where $F_s(\hat{x}) = F_s(\hat{y}) = 1$ is an s-wave form factor. We used $|\Delta_{C_x}| = |\Delta_{C_y}| = 30$ meV at the vortex center in our calculation. Away from the vortex center, CDW has a profile similar to the PDW-driven model:

$$\Delta_C(r) = 30 e^{1-\sqrt{r^2+\xi^2}/\xi} \text{ meV}. \tag{B4}$$

For both PDW-driven and CDW-driven models, we use $|\Delta_D| = 20$ meV far away from the vortex core and $\Delta_D(r,\theta) = 20\frac{r}{\sqrt{r^2+r_0^2}}$ meV near the vortex core. We add one d-wave vortex to a $100a \times 100a$ square lattice with open boundary conditions. $\mathbf{Q_x}/\mathbf{2} = (\frac{2\pi}{8}, 0)$ and $\mathbf{Q_y}/\mathbf{2} = (0, \frac{2\pi}{8})$.

After exact diagonalization, we can easily get on-site LDoS at any energy:

$$\rho(\mathbf{x},\omega) = \sum_{E,\sigma} \delta(\omega - E)\psi^*_E(\mathbf{x};\sigma)\psi_E(\mathbf{x};\sigma), \tag{B5}$$

where E labels all energy levels and $\psi_E(x;\sigma)$ is the wave function for $\mathbf{x}$ site and spin σ at energy level E.

For STM experiments, the LDoS at the oxygen site is actually more important. In our simple, one-band model, we can define a bond LDoS:

$$\rho_\mu(\mathbf{x},\omega) = \sum_{E,\sigma} \delta(\omega - E)(\psi^*_E(\mathbf{x};\sigma)\psi_E(\mathbf{x}+\mu;\sigma) + \psi^*_E(\mathbf{x}+\mu;\sigma)\psi_E(\mathbf{x};\sigma)), \tag{B6}$$

where $\mu = \hat{x}$ or $\hat{y}$.

It is then easy to define an s-wave bond LDoS as

$$\rho_d(\mathbf{x},\omega) = \rho_{\hat{x}}(\mathbf{x},\omega) + \rho_{\hat{y}}(\mathbf{x},\omega) \tag{B7}$$

and a d-wave bond LDoS as

$$\rho_s(\mathbf{x},\omega) = \rho_{\hat{x}}(\mathbf{x},\omega) - \rho_{\hat{y}}(\mathbf{x},\omega). \tag{B8}$$

For a PDW-driven model, we found ρ_d dominates and therefore we only show a d-wave bond DoS in the main text. For our CDW-driven model, it is dominated by s-wave CDW as an input and we show s-wave CDW in the main text.

[1] B. Keimer, S. Kivelson, M. Norman, S. Uchida, and J. Zaanen, Nature (London) **518**, 179 (2015).

[2] A. Shekhter, B. Ramshaw, R. Liang, W. Hardy, D. Bonn, F. F. Balakirev, R. D. McDonald, J. B. Betts, S. C. Riggs, and A. Migliori, Nature (London) **498**, 75 (2013).

[3] L. Zhao, C. Belvin, R. Liang, D. Bonn, W. Hardy, N. Armitage, and D. Hsieh, Nat. Phys. **13**, 250 (2017).

[4] Y. Sato, S. Kasahara, H. Murayama, Y. Kasahara, E.-G. Moon, T. Nishizaki, T. Loew, J. Porras, B. Keimer, T. Shibauchi *et al.*, Nat. Phys. **13**, 1074 (2017).

[5] Matsuda *et al.* (unpublished).

[6] P. Bourges and Y. Sidis, C. R. Phys. **12**, 461 (2011).

[7] C. Varma, Phys. Rev. B **73**, 155113 (2006).

[8] T. P. Croft, E. Blackburn, J. Kulda, R. Liang, D. A. Bonn, W. N. Hardy, and S. M. Hayden, Phys. Rev. B **96**, 214504 (2017).

[9] P. Bourges, Y. Sidis, and L. Mangin-Thro, arXiv:1710.08173.

[10] E. Blackburn, J. Chang, M. Hücker, A. Holmes, N. B. Christensen, R. Liang, D. Bonn, W. Hardy, U. Rütt, O. Gutowski *et al.*, Phys. Rev. Lett. **110**, 137004 (2013).

[11] G. Ghiringhelli, M. Le Tacon, M. Minola, S. Blanco-Canosa, C. Mazzoli, N. Brookes, G. De Luca, A. Frano, D. Hawthorn, F. He *et al.*, Science **337**, 821 (2012).

[12] S. Blanco-Canosa, A. Frano, E. Schierle, J. Porras, T. Loew, M. Minola, M. Bluschke, E. Weschke, B. Keimer, and M. Le Tacon, Phys. Rev. B **90**, 054513 (2014).

[13] W. Tabis, B. Yu, I. Bialo, M. Bluschke, T. Kolodziej, A. Kozlowski, E. Blackburn, K. Sen, E. Forgan, M. v. Zimmermann *et al.*, Phys. Rev. B **96**, 134510 (2017).

[14] T. Wu, H. Mayaffre, S. Krämer, M. Horvatić, C. Berthier, W. Hardy, R. Liang, D. Bonn, and M.-H. Julien, Nature (London) **477**, 191 (2011).

[15] R. Zhou, M. Hirata, T. Wu, I. Vinograd, H. Mayaffre, S. Krämer, A. P. Reyes, P. L. Kuhns, R. Liang, W. Hardy *et al.*, Proc. Natl. Acad. Sci. USA **114**, 13148 (2017).

[16] T. Wu, H. Mayaffre, S. Krämer, M. Horvatić, C. Berthier, P. L. Kuhns, A. P. Reyes, R. Liang, W. Hardy, D. Bonn *et al.*, Nat. Commun. **4**, 2113 (2013).

[17] J. Chang, E. Blackburn, O. Ivashko, A. Holmes, N. B. Christensen, M. Hücker, R. Liang, D. Bonn, W. Hardy, U. Rütt *et al.*, Nat. Commun. **7**, 11494 (2016).

[18] S. Gerber, H. Jang, H. Nojiri, S. Matsuzawa, H. Yasumura, D. Bonn, R. Liang, W. Hardy, Z. Islam, A. Mehta *et al.*, Science **350**, 949 (2015).

[19] H. Jang, W.-S. Lee, H. Nojiri, S. Matsuzawa, H. Yasumura, L. Nie, A. Maharaj, S. Gerber, Y.-J. Liu, A. Mehta *et al.*, Proc. Natl. Acad. Sci. USA **113**, 14645 (2016).

[20] S. E. Sebastian and C. Proust, Annu. Rev. Condens. Matter Phys. **6**, 411 (2015).

[21] S. D. Edkins, A. Kostin, K. Fujita, A. P. Mackenzie, H. Eisaki, S.-I. Uchida, S. Sachdev, M. J. Lawler, E.-A. Kim, J. Davis *et al.*, arXiv:1802.04673.

[22] A. Larkin and I. Ovchinnikov, Sov. Phys. JETP **20**, 762 (1965).

[23] P. Fulde and R. A. Ferrell, Phys. Rev. **135**, A550 (1964).

[24] A. Himeda, T. Kato, and M. Ogata, Phys. Rev. Lett. **88**, 117001 (2002).

[25] J. Tranquada, Nature (London) **375**, 561 (1995).

[26] S. Tajima, T. Noda, H. Eisaki, and S. Uchida, Phys. Rev. Lett. **86**, 500 (2001).

[27] Q. Li, M. Hücker, G. D. Gu, A. M. Tsvelik, and J. M. Tranquada, Phys. Rev. Lett. **99**, 067001 (2007).

[28] E. Berg, E. Fradkin, E.-A. Kim, S. A. Kivelson, V. Oganesyan, J. M. Tranquada, and S. C. Zhang, Phys. Rev. Lett. **99**, 127003 (2007).

[29] E. Berg, E. Fradkin, and S. A. Kivelson, Phys. Rev. B **79**, 064515 (2009).

[30] E. Berg, E. Fradkin, S. A. Kivelson, and J. M. Tranquada, New J. Phys. **11**, 115004 (2009).

[31] D. Agterberg and H. Tsunetsugu, Nat. Phys. **4**, 639 (2008).

[32] E. Berg, E. Fradkin, and S. A. Kivelson, Nat. Phys. **5**, 830 (2009).

[33] S. Baruch and D. Orgad, Phys. Rev. B **77**, 174502 (2008).

[34] R.-H. He, M. Hashimoto, H. Karapetyan, J. Koralek, J. Hinton, J. Testaud, V. Nathan, Y. Yoshida, H. Yao, K. Tanaka *et al.*, Science **331**, 1579 (2011).

[35] P. A. Lee, Phys. Rev. X **4**, 031017 (2014).

[36] S.-S. Lee, P. A. Lee, and T. Senthil, Phys. Rev. Lett. **98**, 067006 (2007).

[37] E. Fradkin, S. A. Kivelson, and J. M. Tranquada, Rev. Mod. Phys. **87**, 457 (2015).

[38] K. Yamada, C. Lee, K. Kurahashi, J. Wada, S. Wakimoto, S. Ueki, H. Kimura, Y. Endoh, S. Hosoya, G. Shirane *et al.*, Phys. Rev. B **57**, 6165 (1998).

[39] A. Beyer, M. Grinolds, M. Teague, S. Tajima, and N.-C. Yeh, Europhys. Lett. **87**, 37005 (2009).

[40] N.-C. Yeh and A. Beyer, Int. J. Mod. Phys. B **23**, 4543 (2009).

[41] M. Zelli, C. Kallin, and A. J. Berlinsky, Phys. Rev. B **86**, 104507 (2012).

[42] M. Norman and J. Davis (unpublished).

[43] F. Yu, M. Hirschberger, T. Loew, G. Li, B. J. Lawson, T. Asaba, J. Kemper, T. Liang, J. Porras, G. S. Boebinger *et al.*, Proc. Natl. Acad. Sci. USA **113**, 12667 (2016).

[44] G. Koren and P. A. Lee, Phys. Rev. B **94**, 174515 (2016).

[45] C. Pépin, V. S. de Carvalho, T. Kloss, and X. Montiel, Phys. Rev. B **90**, 195207 (2014).

[46] Y. Wang, D. F. Agterberg, and A. Chubukov, Phys. Rev. Lett. **114**, 197001 (2015).

[47] D. F. Agterberg, D. S. Melchert, and M. K. Kashyap, Phys. Rev. B **91**, 054502 (2015).

[48] P. Corboz, T. M. Rice, and M. Troyer, Phys. Rev. Lett. **113**, 046402 (2014).

[49] Y. Wang, S. D. Edkins, M. H. Hamidian, J. C. Séamus Davis, E. Fradkin, and S. A. Kivelson, Phys. Rev. B **97**, 174510 (2018).

[50] In momentum space, there are two amplitudes A_a^x and A_a^y at momentum $\mathbf{Q_a}/\mathbf{2}$ which correspond to density waves in x and y bonds, respectively. Here, a denotes x or y: $\mathbf{Q_x}/\mathbf{2} = (\frac{2\pi}{8},0)$ and $\mathbf{Q_y}/\mathbf{2} = (\frac{2\pi}{8},0)$. The definition currently used by the community is to define $A_a^x \pm A_a^y$ as the s/d-wave component. However, under C_4 rotation, A_x^x transforms to A_y^y. Therefore the current definition of s/d-wave form factor is not related to symmetry and generally they should be mixed. An alternative definition of s vs d-wave component is $A_x^x \pm A_y^y$, which is related to the C4 rotation around a particular reference point. However, this definition may not be very useful because if we shift the reference point by half of the period in one direction, what we would define as d wave would become s wave.

[51] There is a redundancy in this definition: we can shift θ_x and ϕ_x (θ_y and ϕ_y) both by π without changing any physical order parameter. Thus ϕ_x (ϕ_y) is determined only up to π without reference to the choice of θ_x (θ_y).

[52] A. Allais and T. Senthil, Phys. Rev. B **86**, 045118 (2012).

[53] L. Wang and O. Vafek, Phys. Rev. B **88**, 024506 (2013).

[54] M. R. Norman, A. H. MacDonald, and H. Akera, Phys. Rev. B **51**, 5927 (1995).

[55] K.-T. Chen and P. A. Lee, Phys. Rev. B **79**, 180510 (2009).

[56] Physically, there is only one electron pocket, the four pockets shown in Fig. 1(c) are copies of the same pocket shifted in momentum, as a consequence of BZ folding.
[57] D. F. Agterberg and J. Garaud, Phys. Rev. B **91**, 104512 (2015).
[58] M. Hamidian, S. D. Edkins, C. K. Kim, J. C. Davis, A. Mackenzie, H. Eisaki, S. Uchida, M. Lawler, E.-A. Kim, S. Sachdev *et al.*, Nat. Phys. **12**, 150 (2016).
[59] T. Wu, H. Mayaffre, S. Krämer, M. Horvatić, C. Berthier, W. Hardy, R. Liang, D. Bonn, and M.-H. Julien, Nat. Commun. **6**, 6438 (2015).
[60] S. E. Sebastian, N. Harrison, and G. G. Lonzarich, Rep. Prog. Phys. **75**, 102501 (2012).
[61] V. Aji and C. M. Varma, Phys. Rev. B **79**, 184501 (2009).